Chapter 4
Results and Discussions

4.1. Introduction

The analytical and the FE formulations are derived for the different non-polynomial shear deformation theories based upon different trigonometric function i.e., the secant function and the inverse hyperbolic sine function in the previous chapter are utilized here to determine the static, dynamic and buckling responses of carbon nanotube reinforced composite and sandwich plate structures. The chapter begins with the analytical modelling followed by the FE modelling of carbon nanotube reinforced composite plates to determine the structural responses due to the action of the mechanical load. Under this part, bending, free vibration, and buckling responses are obtained. The bending analysis of carbon nanotube reinforced composite plates includes transverse deflection resulting from mechanical load, normal stresses, in plane shear stress, and transverse shear stresses resulting from the modifications of the different parametric conditions, which primarily incorporates the variation of the reinforcement distribution pattern of carbon nanotubes across the thickness of the carbon nanotube reinforced composite plate, volume fraction of carbon nanotubes in carbon nanotube reinforced composite plate, and side to thickness ratio. Further, the carbon nanotube reinforced composite plate is studied for free vibration analysis in order to determine the natural frequencies and mode caused by variations in various parametric conditions. These include variations in the reinforcement pattern of carbon nanotubes across the thickness of the carbon nanotube reinforced composite plate, the volume fraction of carbon nanotubes in the carbon nanotube reinforced composite plate, and an array of

other factors. Furthermore, the effect of various parametric conditions, such as varying the reinforcement distribution pattern of carbon nanotubes across the thickness of the carbon nanotube reinforced composite plate, volume fraction of carbon nanotubes in the carbon nanotube reinforced composite plate, and effect of side to thickness ratios on buckling behaviour of the carbon nanotube reinforced composite plate subjected to uniaxial and biaxial compressive load. Next, the analytical and FE modelling of carbon nanotube reinforced sandwich plates is used here to determine the structural responses due to the action of the mechanical load. Different topography in stacking sequence of thee layer sandwich plate is selected here for the analysis. The bending analysis of carbon nanotube reinforced sandwich plates in terms of transverse deflection, normal stresses, in plane shear stresses, and transverse shear stresses resulting from the modifications of the different parametric conditions, such as variation of the reinforcement distribution pattern of carbon nanotubes across the thickness of the carbon nanotube reinforced composite plate, stacking sequence, volume fraction of carbon nanotubes in carbon nanotube reinforced composite plate, and side to thickness ratios are obtained. Further, the free vibration analyses of carbon nanotube reinforced sandwich plates are also studied. In the last part of the chapter, the analytical and FE modelling of carbon nanotube reinforced composite plates resting on the Pasternak's elastic foundation is analysed to determine the structural responses due to the action of the mechanical load. Under this part, bending, free vibration, and buckling responses were recorded. The bending analysis of carbon nanotube reinforced composite plates resting on the Pasternak's elastic foundation incorporates transverse deflection resulting from mechanical load, normal stresses, in plane shear stresses, and transverse shear stresses resulting from the modifications of the different parametric conditions, which primarily incorporates the variation of the reinforcement distribution pattern of carbon

nanotubes across the thickness of the carbon nanotube reinforced composite plate, volume fraction of carbon nanotubes in carbon nanotube reinforced composite plate, Winkler spring constant factor, shear layer constant factor, and side to thickness ratios. Further, the carbon nanotube reinforced composite plate resting on the Pasternak's elastic foundation is studied for the free vibration analysis in order to determine the natural frequencies and mode shapes caused by variations in various parametric conditions. These include variations in the reinforcement pattern of carbon nanotubes across the thickness of the carbon nanotube reinforced composite plate, the volume fraction of carbon nanotubes in the carbon nanotube reinforced composite plate, and an array of other factors. Furthermore, the effect of various parametric conditions, which primarily include varying the reinforcement distribution pattern of carbon nanotubes across the thickness of the carbon nanotube reinforced composite plate, volume fraction of carbon nanotubes in the carbon nanotube reinforced composite plate, and side to thickens, on the buckling load of the carbon nanotube reinforced composite plate resting on the Pasternak's elastic foundation for uniaxial and biaxial compressive load is examined.

The analytical approach by Navier's solution method and then the FE mathematical formulations are developed using MATLAB and implemented to examine the structural responses of the carbon nanotube reinforced composite plate. The solutions obtained are first validated with the available results in literature.

The chapter is divided in several sections and sub sections in which the structural analysis of carbon nanotube reinforced composite plate and sandwich plate analysis is conducted by considering different problems. The analysis starts with the structural analysis of carbon nanotube reinforced composite plate under which bending analysis, followed by free vibration analysis, and buckling analysis. In the bending analysis of

carbon nanotube reinforced composite plate, the bending behaviour of the plate under the action of different loading conditions and parametric conditions are evaluated. The bending analysis includes the transverse deflection, normal stresses, in plane shear stresses, and transverse shear stresses. The section is followed by the free vibration analysis and corresponding mode shapes of carbon nanotube reinforced composite plate. Next, the buckling analysis of carbon nanotube reinforced composite plate under uni-axial and bi-axial loading conditions and corresponding buckling mode shapes are obtained. Further, the structural analysis of carbon nanotube reinforced sandwich plate analysis is conducted by considering different problems which include bending and free vibrational analysis. This section is followed by the structural analysis of carbon nanotube reinforced composite plate resting on Pasternak's elastic foundation. Under this section, bending analysis, free vibration analysis, and buckling analysis are carried out. The last section of the chapter is devoted to a closure.

4.2. Structural analysis of the carbon nanotube reinforced composite plates

The structural analysis of carbon nanotube reinforced composite plate is carried out in this section under which bending analysis, free vibration analysis, and buckling analysis are carried out. In the bending analysis of carbon nanotube reinforced composite plate, the bending behaviour of the plate under the action of different loading conditions and parametric conditions are evaluated. The bending analysis includes the transverse deflection, normal stresses, in plane shear stresses, and transverse shear stresses. The section is followed by the free vibration analysis and corresponding mode shapes of carbon nanotube reinforced composite plate. Next, the buckling analysis under uni-axial and bi-axial loading conditions and corresponding mode shapes are carried out for carbon nanotube reinforced composite plate. Further, simply supported square carbon nanotube reinforced composite plate is selected for the analysis. The

carbon nanotube reinforced composite plate consists of carbon nanotube as the reinforcement fiber which is embedded in PmPV matrix. The material properties are mentioned in the chapter 3, under section 3.10. Non-dimensional parameters selected for the analysis of different numerical results is mentioned under sub section 3.11.

4.2.1. Bending analysis of carbon nanotube reinforced composite plates

In this section, the bending responses of carbon nanotube reinforced composite plates is presented which includes the transverse deflection, normal stresses, in plane shear stresses, and transverse shear stresses under various parametric conditions such as the variation of the reinforcement distribution pattern of carbon nanotubes across the thickness of the carbon nanotube reinforced composite plate, volume fraction of carbon nanotubes in carbon nanotube reinforced composite plate, and side to thickness ratio. As a crucial component of finite element (FE) modelling, the convergence study is essential for assessing the precision and dependability of numerical simulations. It entails looking at how numerical results converge when mesh size or other modelling parameters are adjusted. Engineers and researchers can analyse the degree of mesh refinement necessary to acquire accurate findings and boost their confidence in the FE model's forecasting ability by performing a convergence study. The convergence study guarantees that the FE model adequately depicts the physical behaviour of the system under consideration and is a vital stage in the validation process. Assessing the mesh sensitivity of the FE model is one of the main goals of a convergence research. Mesh sensitivity describes how the model's density and distribution of finite elements affect the numerical results. Because the FE model could miss crucial details or changes in the physical reaction, inaccurate or inadequate meshing might produce erroneous findings. Engineers can assess the amount of mesh refinement required to reach convergence, when further refinement has little to no impact on the numerical solution, by

methodically modifying the mesh and comparing the results. Through this procedure, it is ensured that the FE model properly represents the essential aspects of the system and offers trustworthy forecasts for following studies or design choices. Inadequate mesh resolution may result in modelling mistakes or artefacts, which may be detected through convergence studies. Inaccurate conclusions might occur from the FE model ignoring localised stress concentrations, strain gradients, or other significant phenomena when the mesh is too coarse. Engineers can track the convergence of these values as the mesh is refined and spot areas where the numerical solution deviates from predicted behaviour. With the use of these insights, they may spot modelling flaws, enhance mesh design, and guarantee that the FE model appropriately captures the system's reaction. Convergence studies also offer a quantifiable measurement of the model's sensitivity to mesh refinement, which is a key benefit. Convergence plots may be used by engineers to evaluate the pace of convergence and establish the degree of accuracy of the numerical approach used. This data is essential for evaluating the FE model's dependability and robustness. As the mesh is improved, a faster rate of convergence means that the numerical solution is becoming closer and closer to the precise answer. On the other hand, a slower convergence rate indicates that more work may be required to raise the FE model's correctness. In order to optimise the trade-off between computing resources and solution accuracy, researchers can estimate the computational cost necessary to reach a particular degree of accuracy by understanding the rate of convergence. Convergence studies are also crucial in determining the FE model's overall quality. Engineers can spot any unforeseen or atypical behaviour by comparing the numerical results of several mesh improvements. Significant variances or abnormalities in the findings might be a symptom of modelling mistakes, element distortion, or other problems that require attention. Engineers can carefully analyse

these differences and improve the model by carrying out a convergence study until reliable and physically significant results are reach. This procedure increases the FE model's overall credibility and fosters confidence in its capacity to faithfully capture the behaviour of the system. The convergence investigation is an essential step in confirming the precision and dependability of FE models. Engineers may use it to determine the modelling mistakes, measure the convergence rate, and analyse the overall quality of the numerical findings. Engineers may make sure the FE model properly depicts the physical system under consideration by methodically adjusting the mesh and monitoring the convergence behaviour. The convergence research improves the FE model's capacity for prediction, offers insightful information about the behaviour of the system, and produce trust in the numerical simulations. In the end, the convergence study is a crucial tool for researchers and engineers to produce accurate and trustworthy FE models.

Hence, to validate the FE modeling, the convergence study of the FE solutions for non-dimensional transverse deflection, normal stresses, in plane shear stress, and transverse shear stresses are performed using the secant function based non-polynomial shear deformation theory and are presented in Figure 4.1. For this convergence study of the FE solutions, uniformly distributed carbon nanotube composite plate with the volume fraction of carbon nanotube as 0.17 and span thickness ratio of 10 is selected. The results in the terms of non-dimensional deflection and stresses are obtained for different mesh size varying from 2x2 to 16x16 and are plotted. It is observed from the figure that the results of normalized transverse deflection, normal stresses, in plane shear stress, and transverse shear stresses have converged at a mesh size of 8x8, i.e., 64 numbers of elements. Hence, all the results are obtained at the mesh size of 8x8 if not specified further.

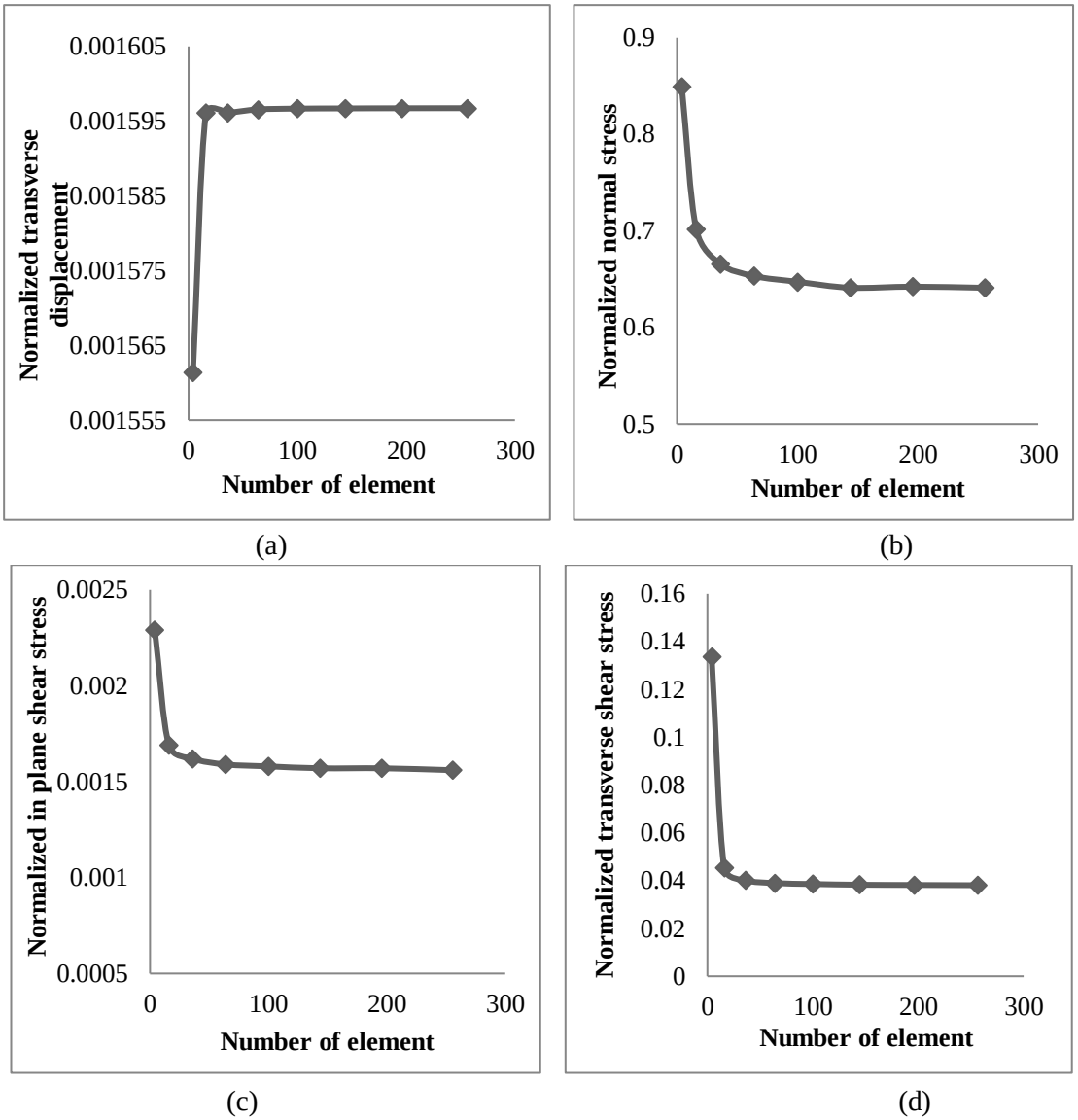

Figure 4.1. Convergence of the FE solutions for (a) non-dimensional transverse deflection, (b) non-dimensional normal stresses, (c) non-dimensional in plane shear stress, (d) non-dimensional transverse shear stresses (S=10)

4.2.1.1. Non-dimensional transverse deflection of the carbon nanotube reinforced composite plate

The non-dimensional transverse deflection of the carbon nanotube reinforced composite plate structure due to mechanical load with the variation of the different parametric conditions such as the reinforcement distribution pattern across the thickness, volume fraction of carbon nanotubes, and side to thickness ratios of carbon nanotube reinforced composite plate are obtained here. For the analysis of non-dimensional transverse deflection of the carbon nanotube reinforced composite plate,

different distribution of carbon nanotube reinforcement pattern is selected from Table 3.1 given in chapter-3 under sub section 3.10.

4.2.1.1.1. Non-dimensional transverse deflection of the carbon nanotube reinforced composite plate under uniformly distributed load

The non-dimensional transverse deflection of the simply supported carbon nanotube reinforced composite plate structure subjected to uniformly distributed load under the variation of the different parametric conditions which mainly incorporates the variation of the reinforcement distribution pattern across the thickness of the carbon nanotube reinforced composite plate, volume fraction of carbon nanotubes, and side to thickness ratios are obtained and is presented in Table 4.1. The analytical and FE results for non-dimensional transverse deflection of carbon nanotube reinforced composite plate structure are obtained in the framework of non-polynomial shear deformation theory based on the secant function and inverse hyperbolic sine function. The material property of CNT selected here, is given in Table 3.3 and the non-dimensional parameter considered here is given in sub section 3.11. The present results are compared with the available FSDT and ANSYS results of Zhu *et al.* (2012), FSDT results of Alibeiglo and Liew (2013) and IHSDT results of Soni et al. (2020) which show that the present results are agreed well with the existing results. From the table, it is observed that the non-dimensional transverse deflection of the carbon nanotube reinforced composite plate subjected to uniformly distributed load varies in the same way as the span thickness ratio by considering all other factors to be constraint. Similarly, if all other factors are kept constraint and the effect of volume fraction of CNTs is observed, it can be seen clearly that by increasing the volume fraction of carbon nanotubes in the carbon nanotube reinforced composite plate, the non-dimensional transverse deflection decreases. In the similar way, for a particular volume fraction of CNTs and span

thickness ratios, the non-dimensional transverse deflection due to transversely applied uniformly distributed load is minimum for FG-X distribution and maximum for FG-O distribution. The ascending order of the resistance to the transverse deflection for a particular volume fraction of CNTs and span thickness ratio is FG-X followed by UD, FG-V and FG-O distributions. The descending order of the plate stiffness for a particular volume fraction of CNTs and span thickness ratio is FG-X followed by UD, FG-V and FG-O distributions.

4.2.1.1.2. Non-dimensional transverse deflection of the carbon nanotube reinforced composite plate under sinusoidal load.

The non-dimensional transverse deflection of the carbon nanotube reinforced composite plate subjected to sinusoidal load is presented in Table 4.2 and detailed analyses for different parametric conditions are carried out. For the analysis of non-dimensional transverse deflection of the simply supported carbon nanotube reinforced composite plate, different distribution of carbon nanotube reinforcement pattern is selected from Table 3.1. The material property selected here, is given in Table 3.3 and the non-dimensional parameter selected from sub section 3.11. In the table, the analytical and FE results are presented which are based on non-polynomial shear deformation theories with the secant function and inverse hyperbolic sine function. The present results are compared with the available results of Soni et al. (2020) which show that the present results are synchronizing well with the published results. From the table it is also observed that the transverse deflection of the carbon nanotube reinforced composite plate subjected to sinusoidal distributed load varies in the same way as the span thickness ratio by considering all other factors constraint. Similarly, if all other factors are kept constraint and only the effect of volume fraction of CNTs is observed, it can be simply observed that by increasing the volume fraction of carbon nanotubes in

the carbon nanotube reinforced composite plate, the non-dimensional transverse deflection decreases. In the same way if one can consider a particular volume fraction of CNTs and span thickness ratio, the non- dimensional transverse deflection due to transversely applied uniformly distributed load is minimum for FG-X distribution and maximum for FG-O distribution. The increasing order of the resistance to the transverse deflection for a particular volume fraction of CNTs and span thickness ratio is FG-X and is followed by UD, FG-V and FG-O distributions. The reducing order of the plate stiffness for a particular volume fraction of CNTs and span thickness ratio is FG-X followed by UD, FG-V and FG-O distributions.

4.2.1.2. Non-dimensional stress analysis of the carbon nanotube reinforced composite plate

In this section, the non-dimensional stress analysis of the simply supported carbon nanotube reinforced composite plate for different parametric conditions is discussed in detail. The analytical approach and FE model is used to analyse the effect of the different span thickness ratios, volume fraction of CNTs, and distribution of CNTs on the stress distribution of the carbon nanotube reinforcement composite plate. Four different types of CNTs reinforcement distribution such as, uniformly distribution (UD) and three types of functionally graded (FG) i.e. FG-O, FG-X and FG-V are selected here for the analysis. For the analysis of non-dimensional stresses of the carbon nanotube reinforced composite plate, different distribution of carbon nanotube reinforcement pattern is selected from Table 3.1. The material property of carbon nanotubes and PmPV matrix, selected here is given in Table 3.3 and the non-dimensional parameter selected from sub section 3.11. Here, the efforts are made to achieve the best possible arrangement for the reinforcement distribution that will produce the improved stress distribution responses for the functionally graded CNTs

reinforced composite plate. The analytical solution and FE results are based on the non-polynomial shear deformation theories with different trigonometric functions i.e., secant function and inverse hyperbolic sine function.

4.2.1.2.1 Non-dimensional normal stress distribution of carbon nanotube reinforced composite plate

The non-dimensional normal stress (σ_{xx}) distribution due to sinusoidal load on the simply supported carbon nanotube reinforced composite plate is presented in Table 4.3. The results for the non-dimensional normal stresses of a carbon nanotube reinforced composite plate were obtained using analytical and FE modelling within the framework of non-polynomial shear deformation theory based on the secant function and inverse hyperbolic sine function. The present results are compared with the IHSDT results of Soni et al. (2020) results which show that the results synchronize well with the present results. The effect of the different parametric conditions on the on normal stresses is observed from the table given below. The normal stress varies inversely with the span thickness ratios by considering all other factors to be constraint. Similarly, for a particular volume fraction of CNTs and span thickness ratio, the normal stress due to transverse load is minimum for FG-O distribution and maximum for FG-V distribution. The ascending order of the normal stresses for a particular volume fraction of CNTs and span thickness ratio is FG-O followed by UD, FG-X and FG-V distributions.

Table 4.1: Dimensionless transverse deflection of carbon nanotube reinforced composite plate subjected to uniformly distributed load

V^*_{CNT}	*b/h*	Distribution	Present[@]	Present[*]	Present[$]	Present[&]	Zhu *et al.* (2012)[*]	Zhu *et al.* (2012)[#]	Alibeiglo and Liew (2013)	Soni *et al.* (2020)
0.11	10	UD	3.670×10^{-3}	3.649×10^{-3}	3.716×10^{-3}	3.659×10^{-3}	3.739×10^{-3}	3.739×10^{-3}	3.617×10^{-3}	3.649×10^{-3}
		FG-V	4.398×10^{-3}	4.384×10^{-3}	4.446×10^{-3}	4.426×10^{-3}	4.466×10^{-3}	4.461×10^{-3}	4.455×10^{-3}	4.384×10^{-3}
		FG-O	5.482×10^{-3}	5.443×10^{-3}	5.429×10^{-3}	5.439×10^{-3}	5.230×10^{-3}	5.216×10^{-3}	-	5.443×10^{-3}
		FG-X	3.126×10^{-3}	3.046×10^{-3}	3.140×10^{-3}	3.115×10^{-3}	3.177×10^{-3}	3.176×10^{-3}	-	3.046×10^{-3}
	20	UD	3.609×10^{-2}	3.608×10^{-2}	3.627×10^{-2}	3.620×10^{-2}	3.628×10^{-2}	3.629×10^{-2}	3.621×10^{-2}	3.608×10^{-2}
		FG-V	4.885×10^{-2}	4.862×10^{-2}	4.879×10^{-2}	4.872×10^{-2}	4.879×10^{-2}	4.876×10^{-2}	4.872×10^{-2}	4.862×10^{-2}
		FG-O	6.258×10^{-2}	6.253×10^{-2}	6.242×10^{-2}	6.250×10^{-2}	6.155×10^{-2}	6.136×10^{-2}	-	6.253×10^{-2}
		FG-X	2.684×10^{-2}	2.665×10^{-2}	2.695×10^{-2}	2.685×10^{-2}	2.701×10^{-2}	2.703×10^{-2}	-	2.665×10^{-2}
	50	UD	1.1556	1.1554	1.1556	1.1552	1.155	1.1550	1.1549	1.1554
		FG-V	1.6358	1.6536	1.6533	1.6529	1.653	1.6520	1.6524	1.6536
		FG-O	2.1638	2.1637	2.1617	2.1623	2.157	2.1500	-	2.1637
		FG-X	0.7900	0.7899	0.7910	0.7904	0.7900	0.7915	-	0.7899
0.14	10	UD	3.267×10^{-3}	3.201×10^{-3}	3.271×10^{-3}	3.250×10^{-3}	3.306×10^{-3}	3.305×10^{-3}	3.295×10^{-3}	3.201×10^{-3}
		FG-V	3.854×10^{-3}	3.801×10^{-3}	3.865×10^{-3}	3.845×10^{-3}	3.894×10^{-3}	3.889×10^{-3}	3.883×10^{-3}	3.801×10^{-3}
		FG-O	4.726×10^{-3}	4.689×10^{-3}	4.683×10^{-3}	4.686×10^{-3}	4.525×10^{-3}	4.512×10^{-3}	-	4.689×10^{-3}
		FG-X	2.840×10^{-3}	2.736×10^{-3}	2.824×10^{-3}	2.800×10^{-3}	2.844×10^{-3}	2.842×10^{-3}	-	2.736×10^{-3}
	20	UD	2.976×10^{-2}	2.971×10^{-2}	2.99×10^{-2}	2.983×10^{-2}	3.001×10^{-2}	3.002×10^{-2}	2.990×10^{-2}	2.971×10^{-2}
		FG-V	4.001×10^{-2}	3.995×10^{-2}	4.012×10^{-2}	4.005×10^{-2}	4.025×10^{-2}	4.021×10^{-2}	4.013×10^{-2}	3.995×10^{-2}
		FG-O	5.140×10^{-2}	5.137×10^{-2}	5.129×10^{-2}	5.134×10^{-2}	5.070×10^{-2}	5.053×10^{-2}	-	5.137×10^{-2}
		FG-X	2.230×10^{-2}	2.229×10^{-2}	2.254×10^{-2}	2.246×10^{-2}	2.256×10^{-2}	2.258×10^{-2}	-	2.229×10^{-2}
	50	UD	0.9240	0.9140	0.9151	0.9147	0.9175	0.9182	0.9174	0.9140
		FG-V	1.3240	1.3210	1.3211	1.3208	1.3260	1.3250	1.3250	1.3210
		FG-O	1.7378	1.7375	1.7359	1.7363	1.7380	1.7320	-	1.7375
		FG-X	0.6258	0.6252	0.6261	0.6256	0.6271	0.6284	-	0.6252

	10	UD	2.372×10^{-3}	2.338×10^{-3}	2.380×10^{-3}	2.367×10^{-3}	2.394×10^{-3}	2.394×10^{-3}	2.383×10^{-3}	2.338×10^{-3}
		FG-V	2.894×10^{-3}	2.822×10^{-3}	2.858×10^{-3}	2.846×10^{-3}	2.864×10^{-3}	2.861×10^{-3}	2.854×10^{-3}	2.822×10^{-3}
		FG-O	3.520×10^{-3}	3.466×10^{-3}	3.464×10^{-3}	3.464×10^{-3}	3.378×10^{-3}	3.368×10^{-3}	-	3.466×10^{-3}
		FG-X	2.001×10^{-3}	1.981×10^{-3}	2.028×10^{-3}	2.014×10^{-3}	2.012×10^{-3}	2.011×10^{-3}	-	1.981×10^{-3}
0.17	20	UD	2.347×10^{-2}	2.336×10^{-2}	2.348×10^{-2}	2.344×10^{-2}	2.348×10^{-2}	2.349×10^{-2}	2.340×10^{-2}	2.336×10^{-2}
		FG-V	3.178×10^{-2}	3.166×10^{-2}	3.176×10^{-2}	3.172×10^{-2}	3.174×10^{-2}	3.171×10^{-2}	3.166×10^{-2}	3.166×10^{-2}
		FG-O	4.120×10^{-2}	4.061×10^{-2}	4.057×10^{-2}	4.058×10^{-2}	4.020×10^{-2}	4.007×10^{-2}	-	4.061×10^{-2}
		FG-X	1.754×10^{-2}	1.714×10^{-2}	1.751×10^{-2}	1.746×10^{-2}	1.737×10^{-2}	1.738×10^{-2}	-	1.714×10^{-2}
	50	UD	0.7528	0.7526	0.7527	0.7525	0.7515	0.7521	0.7514	0.7526
		FG-V	1.0830	1.0829	1.0826	1.0824	1.0820	1.0810	1.0780	1.0829
		FG-O	1.4200	1.4182	1.4171	1.4117	1.4160	1.4110	-	1.4182
		FG-X	0.5152	0.515	0.5153	0.5150	0.5130	0.5140	-	0.5150

Present[@]- Analytical non-polynomial shear deformation theory based on secant function.
Present[*]- Analytical non-polynomial shear deformation theory based on inverse hyperbolic sine function.
Present[$]- FE modeling using non-polynomial shear deformation theory based on secant function.
Present[&]- FE modeling using non-polynomial shear deformation theory based on inverse hyperbolic sine function.
[*] FSDT, [#] ANSYS

Table 4.2: Dimensionless transverse deflection of carbon nanotube reinforced composite plate subjected to sinusoidal loading condition

V^*_{CNT}	b/h	Distribution	Present[@]	Present[*]	Present[$]	Present[&]	Soni *et al.* (2020)
0.11	10	UD	2.490×10^{-3}	2.461×10^{-3}	2.50×10^{-3}	2.49×10^{-3}	2.461×10^{-3}
		FG-V	2.951×10^{-3}	2.919×10^{-3}	2.96×10^{-3}	2.951×10^{-3}	2.919×10^{-3}
		FG-O	3.560×10^{-3}	3.592×10^{-3}	3.59×10^{-3}	3.56×10^{-3}	3.592×10^{-3}
		FG-X	2.122×10^{-3}	2.075×10^{-3}	2.14×10^{-3}	2.122×10^{-3}	2.075×10^{-3}
	20	UD	2.468×10^{-2}	2.461×10^{-2}	2.47×10^{-2}	2.468×10^{-2}	2.461×10^{-2}
		FG-V	3.257×10^{-2}	3.25×10^{-2}	3.26×10^{-2}	3.257×10^{-2}	3.25×10^{-2}
		FG-O	4.110×10^{-2}	4.138×10^{-2}	4.13×10^{-2}	4.11×10^{-2}	4.138×10^{-2}
		FG-X	1.865×10^{-2}	1.851×10^{-2}	1.87×10^{-2}	1.865×10^{-2}	1.851×10^{-2}
	50	UD	0.7900	0.7910	0.7910	0.7900	0.7910
		FG-V	1.1050	1.1060	1.106	1.1050	1.1060
		FG-O	1.4300	1.4310	1.4308	1.4300	1.4310
		FG-X	0.5532	0.5530	0.5538	0.5532	0.5530
0.14	10	UD	2.220×10^{-3}	2.175×10^{-3}	2.22×10^{-3}	2.220×10^{-3}	2.175×10^{-3}
		FG-V	2.593×10^{-3}	2.546×10^{-3}	2.59×10^{-3}	2.593×10^{-3}	2.546×10^{-3}
		FG-O	3.100×10^{-3}	3.117×10^{-3}	3.1×10^{-3}	3.100×10^{-3}	3.117×10^{-3}
		FG-X	1.920×10^{-3}	1.870×10^{-3}	1.93×10^{-3}	1.920×10^{-3}	1.870×10^{-3}
	20	UD	2.062×10^{-2}	2.048×10^{-2}	2.06×10^{-2}	2.062×10^{-2}	2.048×10^{-2}
		FG-V	2.710×10^{-2}	2.695×10^{-2}	2.70×10^{-2}	2.710×10^{-2}	2.695×10^{-2}
		FG-O	3.423×10^{-2}	2.430×10^{-2}	3.42×10^{-2}	3.423×10^{-2}	2.430×10^{-2}
		FG-X	1.580×10^{-2}	1.562×10^{-2}	1.58×10^{-2}	1.580×10^{-2}	1.562×10^{-2}
	50	UD	0.6352	0.6345	0.6349	0.6352	0.6345
		FG-V	0.8942	0.8932	0.8935	0.8942	0.8932
		FG-O	1.1620	1.1618	1.1610	1.1620	1.1618
		FG-X	0.4439	0.4431	0.4439	0.4439	0.4431
0.17	10	UD	1.600×10^{-3}	1.576×10^{-3}	1.60×10^{-3}	1.600×10^{-3}	1.576×10^{-3}
		FG-V	1.898×10^{-3}	1.876×10^{-3}	1.90×10^{-3}	1.898×10^{-3}	1.876×10^{-3}
		FG-O	2.280×10^{-3}	2.290×10^{-3}	2.29×10^{-3}	2.280×10^{-3}	2.290×10^{-3}
		FG-X	1.376×10^{-3}	1.344×10^{-3}	1.37×10^{-3}	1.376×10^{-3}	1.344×10^{-3}
	20	UD	1.592×10^{-2}	1.591×10^{-2}	1.59×10^{-2}	1.592×10^{-2}	1.591×10^{-2}
		FG-V	2.111×10^{-2}	2.112×10^{-2}	2.11×10^{-2}	2.111×10^{-2}	2.112×10^{-2}
		FG-O	2.685×10^{-2}	2.686×10^{-2}	2.68×10^{-2}	2.685×10^{-2}	2.686×10^{-2}
		FG-X	1.200×10^{-2}	1.200×10^{-2}	1.21×10^{-2}	1.200×10^{-2}	1.200×10^{-2}
	50	UD	0.5117	0.5142	0.5145	0.5117	0.5142
		FG-V	0.7194	0.7225	0.7226	0.7194	0.7225
		FG-O	0.9392	0.9381	0.9376	0.9392	0.9381
		FG-X	0.3588	0.3585	0.3588	0.3588	0.3585

Present[@]- Analytical non-polynomial shear deformation theory based on secant function.
Present[*]- Analytical non-polynomial shear deformation theory based on inverse hyperbolic sine function.
Present[$]- FE modeling using non-polynomial shear deformation theory based on secant function.
Present[&]- FE modeling using non-polynomial shear deformation theory based on inverse hyperbolic sine function.

Table 4.3: Non-dimensional normal stresses (σ_{xx}) of carbon nanotube reinforced composite plate

V^*_{CNT}	*b/h*	Distribution	Present[@]	Present[*]	Present[$]	Present[&]	Soni *et al.* (2020)
0.11	10	UD	0.6527	0.6571	0.6641	0.6571	0.6571
		FG-V	1.2350	1.2780	1.2567	1.2435	1.2780
		FG-O	0.0413	0.0438	0.0447	0.0448	0.0438
		FG-X	0.9133	0.9437	0.9171	0.9015	0.9437
	20	UD	0.5915	0.5978	0.6068	0.6054	0.5978
		FG-V	1.1170	1.1290	1.1465	1.1437	1.1290
		FG-O	0.0361	0.0374	0.0383	0.0384	0.0374
		FG-X	0.8069	0.8155	0.8251	0.8213	0.8155
	50	UD	0.5730	0.5751	0.5889	0.5887	0.5751
		FG-V	1.0839	1.0860	1.1119	1.1150	1.0860
		FG-O	0.0346	0.0355	2.1344	0.0364	0.0355
		FG-X	0.7750	0.7776	0.7958	0.7952	0.7776
0.14	10	UD	0.6838	0.7092	0.6915	0.6824	0.7092
		FG-V	1.3060	1.3552	1.3220	1.3050	1.3552
		FG-O	0.0348	0.0374	0.0382	0.0382	0.0374
		FG-X	0.9629	0.9980	0.9629	0.9444	0.9980
	20	UD	0.6046	0.6116	0.6195	0.6176	0.6116
		FG-V	1.1540	1.1670	1.1823	1.1789	1.1670
		FG-O	0.0300	0.0310	0.0317	0.0318	0.0310
		FG-X	0.8251	0.8349	0.8433	0.8390	0.8349
	50	UD	0.5816	0.5828	0.5965	0.5962	0.5828
		FG-V	1.1102	1.1120	1.1378	1.1373	1.1120
		FG-O	0.0280	0.0291	0.0298	0.0298	0.0291
		FG-X	0.7847	0.7864	0.8046	0.8039	0.7864
0.17	10	UD	0.6504	0.6700	0.6599	0.6532	0.6700
		FG-V	1.2370	1.2730	1.2552	1.2429	1.2730
		FG-O	0.0326	0.0357	0.0364	0.0364	0.0357
		FG-X	0.9100	0.9396	0.9208	0.9077	0.9396
	20	UD	0.5905	0.5957	0.6049	0.6035	0.5957
		FG-V	1.1220	1.1306	1.1484	1.1459	1.1306
		FG-O	0.0281	0.0302	0.0309	0.0310	0.0302
		FG-X	0.8050	0.8133	0.8248	0.8278	0.8133
	50	UD	0.5732	0.5739	0.5877	0.5875	0.5739
		FG-V	1.0893	1.0889	1.1151	1.1147	1.0889
		FG-O	0.0268	0.0286	0.0293	0.0293	0.0286
		FG-X	0.7746	0.7760	0.7944	0.7940	0.7760

Present[@]- Analytical non-polynomial shear deformation theory based on secant function.
Present[*]- Analytical non-polynomial shear deformation theory based on inverse hyperbolic sine function.
Present[$]- FE modeling using non-polynomial shear deformation theory based on secant function.
Present[&]- FE modeling using non-polynomial shear deformation theory based on inverse hyperbolic sine function.

The variation of non-dimensional axial stresses (σ_{xx}) with normalized thickness for a particular volume fraction of CNTs i.e. 0.17 is shown in Figure 4.2. The analytical results of non-dimensional axial stresses of carbon nanotube reinforced composite plate are obtained using the non-polynomial shear deformation theory based on the secant function. Here, simply supported square carbon nanotube reinforced composite plate is subjected to the sinusoidal loading condition with span thickness ratio of 50 is considered for the analysis. It is observed from the figure that for the symmetrical distribution i.e. FG-O, FG-X, and UD of the CNTs in the composite plate, the distribution of the non-dimensional axial stress is anti-symmetrical along the central axis. In FG-V CNTRC plate, CNTs are maximum at the top face of the plate and minimum at the bottom face of the plate due to which, non-dimensional axial stresses are close to zero at the bottom of the plate and maximum at the top face of the plate. Similarly, in the case of FG-O distribution, the presence of CNTs are minimum at the top and bottom face of the plate due to which the non-dimensional axial stresses are close to zero at the top and bottom of the plate. In case of the symmetrical distribution of the CNTs, the value of the non-dimensional axial stresses is zero at the mid plane. It is also observed that the normal stresses for particular span thickness ratio and volume fraction of the CNTs, FG-O distribution show minimum flexural rigidity as compared to the FG-V which show maximum flexural rigidity.

The variation of the non-dimensional axial stresses (σ_{xx}) with the span thickness ratio is shown in the Figure 4.3. This investigation is done through the application of analytical modelling of carbon nanotube reinforced composite plate within the context of non-polynomial shear deformation theory based on the secant function.

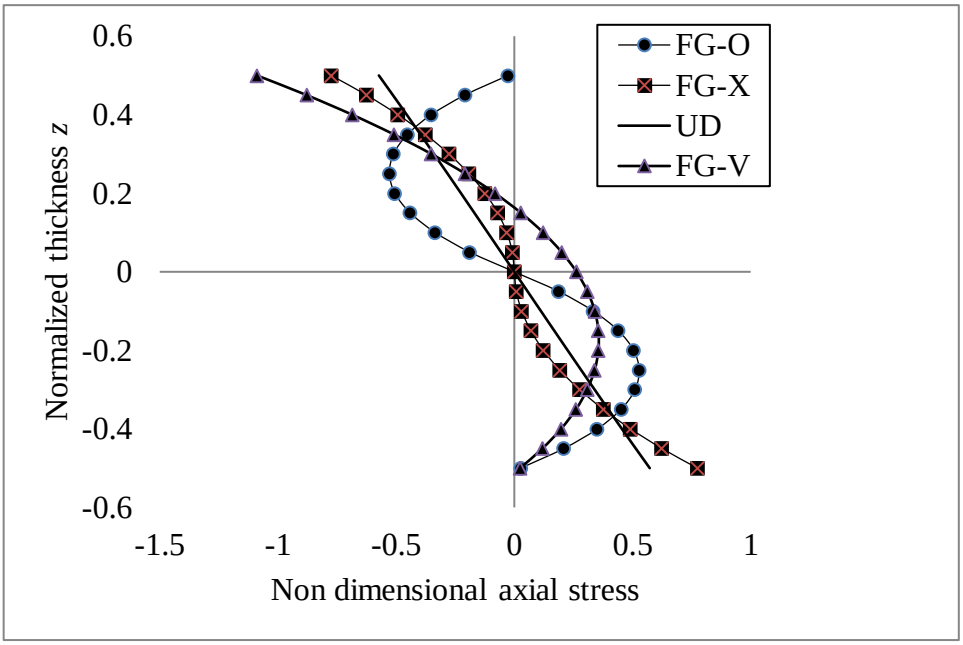

Figure 4.2. Variation of non-dimensional axial stresses (σ_{xx}) with normalized thickness

A simply supported square carbon nanotube reinforced composite plate subjected to sinusoidal loading condition is considered for the analysis, with the volume fraction of the CNTs as 0.11. It is observed from the analysis that the non-dimensional axial stress is decreased as span thickness ratio increases. The non-dimensional axial stresses are maximum for FG-V distribution and minimum for FG-O distribution.

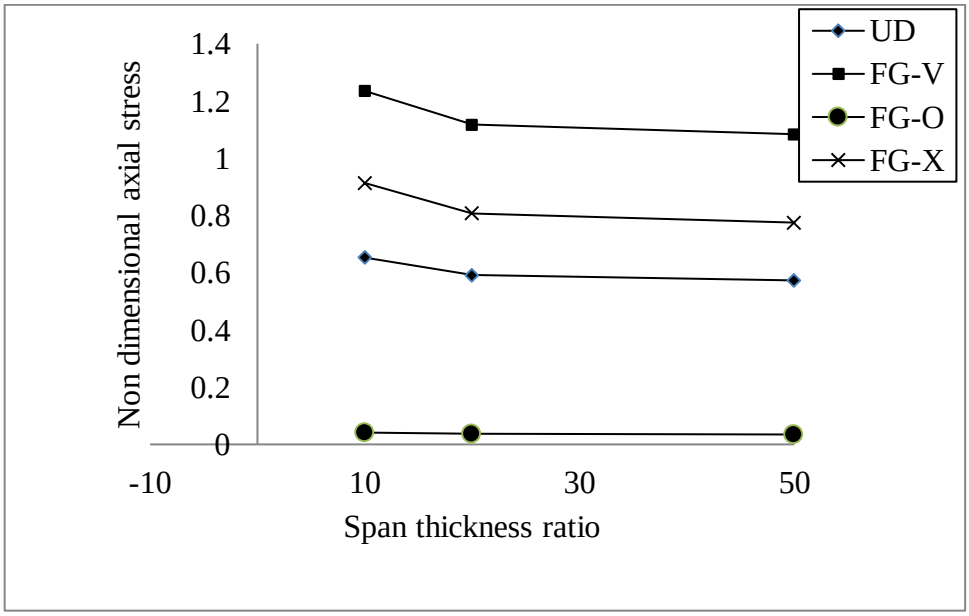

Figure 4.3. Variation of non-dimensional axial stresses (σ_{xx}) with different span thickness ratios

4.2.1.2.2. Non-dimensional in plane shear stress distribution of carbon nanotube reinforced composite plate

In Table 4.4 the in plane shear stresses (τ_{xy}) are present at point (a, b, $h/2$) of carbon nanotube reinforced composite plate. The analysis is conducted for simply supported carbon nanotube reinforced composite plate subjected to sinusoidal loading condition. The detailed parametric study is carried out which includes the different distributions of carbon nanotubes, span thickness ratio and volume fraction of the carbon nanotubes. For the analysis of the in plane shear stresses analytical method is adopted in the framework of the non-polynomial shear deformation theory based on the secant function and inverse hyperbolic sine function. For the validation of the mathematical model developed with the analytical method, numerical solution is developed with the help of finite element method in the same framework and both the results i.e. obtained through analytical and finite element method are compared with the available result of the literature. In the table fourth column represents the present result obtained by the analytical solution in the framework of non-polynomial shear deformation theory based on secant function. Whereas fifth column represents the present result obtained by the analytical solution in the framework of non-polynomial deformation theory based on inverse hyperbolic sine function. Similarly the sixth column represents the present result obtained using numerical solution based upon finite element method in the framework of non-polynomial shear deformation theory based upon the secant function and seventh column represents the present result obtained using the numerical solution based upon finite element method in the framework of non-polynomial shear deformation theory based upon the inverse hyperbolic sine function. Eighth column represents the results presented by Soni et al. (2020) in the literature. All the presented results synchronise well with each other along with the Soni et al. (2020) results. It is observed from the

table that for a particular CNTs distribution and volume fraction of the CNTs the non-dimensional in plane shear stresses decreases with the increase in the span thickness ratio. Similarly, for a constant value of the span thickness ratio, as the value of the volume fraction of carbon nanotubes in carbon nanotube reinforced composite plate increases, the non-dimensional in plane shear stresses decreases. For a particular volume fraction of carbon nanotube and span thickness ratio, FG-O distribution show maximum in plane shear stresses as compared to the FG-X which show minimum in plane shear stresses. The increasing order of in plane shear stresses for different carbon nanotube distribution for a particular volume fraction of carbon nanotube and span thickness ratio is FG-X, UD, FG-V and FG-O.

Table 4.4: In plane shear stresses (τ_{xy}) of carbon nanotube reinforced composite plate

V^*_{CNT}	*b/h*	Distribution	Present[@]	Present[*]	Present[$]	Present[&]	Soni *et al.* (2020)
0.11	10	UD	1.550×10^{-2}	1.540×10^{-2}	1.57×10^{-2}	1.560×10^{-2}	1.540×10^{-2}
		FG-V	2.010×10^{-2}	1.848×10^{-2}	2.04×10^{-2}	2.030×10^{-2}	1.848×10^{-2}
		FG-O	2.140×10^{-2}	2.178×10^{-2}	2.22×10^{-2}	2.178×10^{-2}	2.178×10^{-2}
		FG-X	1.410×10^{-2}	1.396×10^{-2}	1.43×10^{-2}	1.420×10^{-2}	1.396×10^{-2}
	20	UD	1.130×10^{-2}	1.133×10^{-2}	1.16×10^{-2}	1.150×10^{-2}	1.133×10^{-2}
		FG-V	1.500×10^{-2}	1.498×10^{-2}	1.61×10^{-2}	1.610×10^{-2}	1.498×10^{-2}
		FG-O	1.760×10^{-2}	1.762×10^{-2}	1.80×10^{-2}	1.800×10^{-2}	1.762×10^{-2}
		FG-X	0.940×10^{-2}	0.973×10^{-2}	0.96×10^{-2}	0.950×10^{-2}	0.973×10^{-2}
	50	UD	1.010×10^{-2}	1.008×10^{-2}	1.03×10^{-2}	1.030×10^{-2}	1.008×10^{-2}
		FG-V	1.400×10^{-2}	1.393×10^{-2}	1.48×10^{-2}	1.480×10^{-2}	1.393×10^{-2}
		FG-O	1.650×10^{-2}	1.638×10^{-2}	1.65×10^{-2}	1.680×10^{-2}	1.638×10^{-2}
		FG-X	0.800×10^{-2}	0.797×10^{-2}	0.82×10^{-2}	0.810×10^{-2}	0.797×10^{-2}
0.14	10	UD	1.387×10^{-2}	1.387×10^{-2}	1.41×10^{-2}	1.400×10^{-2}	1.387×10^{-2}
		FG-V	1.846×10^{-2}	1.598×10^{-2}	1.89×10^{-2}	1.870×10^{-2}	1.598×10^{-2}
		FG-O	1.830×10^{-2}	1.872×10^{-2}	1.91×10^{-2}	1.910×10^{-2}	1.872×10^{-2}
		FG-X	1.347×10^{-2}	1.336×10^{-2}	1.37×10^{-2}	1.350×10^{-2}	1.336×10^{-2}
	20	UD	0.966×10^{-2}	0.968×10^{-2}	0.99×10^{-2}	0.980×10^{-2}	0.968×10^{-2}
		FG-V	1.390×10^{-2}	1.247×10^{-2}	1.43×10^{-2}	1.420×10^{-2}	1.247×10^{-2}
		FG-O	1.440×10^{-2}	1.459×10^{-2}	1.49×10^{-2}	1.490×10^{-2}	1.459×10^{-2}
		FG-X	0.845×10^{-2}	0.845×10^{-2}	0.86×10^{-2}	0.860×10^{-2}	0.845×10^{-2}
	50	UD	0.840×10^{-2}	0.840×10^{-2}	0.86×10^{-2}	0.860×10^{-2}	0.840×10^{-2}
		FG-V	1.250×10^{-2}	1.140×10^{-2}	1.29×10^{-2}	1.890×10^{-2}	1.140×10^{-2}
		FG-O	1.336×10^{-2}	1.337×10^{-2}	1.37×10^{-2}	1.370×10^{-2}	1.337×10^{-2}

0.17	10	FG-X	0.693×10^{-2}	0.694×10^{-2}	0.71×10^{-2}	0.710×10^{-2}	0.694×10^{-2}
		UD	1.565×10^{-2}	1.574×10^{-2}	1.6×10^{-2}	1.590×10^{-2}	1.574×10^{-2}
		FG-V	2.191×10^{-2}	1.798×10^{-2}	2.25×10^{-2}	2.240×10^{-2}	1.798×10^{-2}
		FG-O	2.030×10^{-2}	2.071×10^{-2}	2.11×10^{-2}	2.110×10^{-2}	2.071×10^{-2}
	20	FG-X	1.580×10^{-2}	1.577×10^{-2}	1.61×10^{-2}	1.600×10^{-2}	1.577×10^{-2}
		UD	1.155×10^{-2}	1.164×10^{-2}	1.19×10^{-2}	1.190×10^{-2}	1.164×10^{-2}
		FG-V	1.790×10^{-2}	1.469×10^{-2}	1.79×10^{-2}	1.790×10^{-2}	1.469×10^{-2}
		FG-O	1.698×10^{-2}	1.698×10^{-2}	1.74×10^{-2}	1.740×10^{-2}	1.698×10^{-2}
	50	FG-X	1.060×10^{-2}	1.061×10^{-2}	1.08×10^{-2}	1.080×10^{-2}	1.061×10^{-2}
		UD	1.033×10^{-2}	1.040×10^{-2}	1.06×10^{-2}	1.060×10^{-2}	1.040×10^{-2}
		FG-V	1.060×10^{-2}	1.370×10^{-2}	1.66×10^{-2}	1.660×10^{-2}	1.370×10^{-2}
		FG-O	1.588×10^{-2}	1.588×10^{-2}	1.63×10^{-2}	1.630×10^{-2}	1.588×10^{-2}
		FG-X	0.902×10^{-2}	0.903×10^{-2}	0.92×10^{-2}	0.920×10^{-2}	0.903×10^{-2}

Present[@]- Analytical non-polynomial shear deformation theory based on secant function.
Present[*]- Analytical non-polynomial shear deformation theory based on inverse hyperbolic sine function.
Present[$]- FE modeling using non-polynomial shear deformation theory based on secant function.
Present[&]- FE modeling using non-polynomial shear deformation theory based on inverse hyperbolic sine function.

4.2.1.2.3. Non-dimensional transverse shear stress distribution of carbon nanotube reinforced composite plate

Table 4.5 presents the transverse shear stresses (τ_{xz}) at point (0, 0, $h/2$) of carbon nanotube reinforced composite plate. The analysis is conducted for simply supported carbon nanotube reinforced composite plate subjected to sinusoidal loading condition. The detailed parametric study is carried out which includes the different distributions of carbon nanotubes, span thickness ratio and volume fraction of the carbon nanotubes. For the analysis of the transverse shear stresses analytical method is adopted in the framework of the non-polynomial shear deformation theory based on the secant function and inverse hyperbolic sine function. For the validation of the mathematical model developed with the analytical method, numerical solution is developed with the help of finite element method in the same framework and both the results i.e. obtained through analytical and finite element method are compared with the available result of the literature. In the table fourth column represents the present result obtained by the analytical solution in the framework of non-polynomial shear deformation theory based

on secant function. Whereas fifth column represents the present result obtained by the analytical solution in the framework of non-polynomial deformation theory based on inverse hyperbolic sine function. Similarly the sixth column represents the present result obtained using numerical solution based upon finite element method in the framework of non-polynomial shear deformation theory based upon the secant function and seventh column represents the present result obtained using the numerical solution based upon finite element method in the framework of non-polynomial shear deformation theory based upon the inverse hyperbolic sine function. Eighth column represents the results presented by Soni et al. (2020) in the literature. All the presented results synchronise well with each other along with the Soni et al. (2020) results. It is observed from the table that the non-dimensional transverse shear stress decreases with the increase in the span thickness ratio, for a particular CNTs distribution and volume fraction of the CNTs. The FG-O distribution show maximum non-dimensional transverse shear stress as compared with the FG-X which show minimum non-dimensional transverse shear stresses.

Table 4.5: Transverse shear stresses (τ_{xz}) of carbon nanotube reinforced composite plate

V^*_{CNT}	*b/h*	Distribution	Present[@]	Present[*]	Present[$]	Present[&]	Soni *et al.* (2020)
0.11	10	UD	3.510×10^{-2}	3.921×10^{-2}	3.590×10^{-2}	3.840×10^{-2}	3.921×10^{-2}
		FG-V	4.350×10^{-2}	4.882×10^{-2}	4.450×10^{-2}	4.770×10^{-2}	4.882×10^{-2}
		FG-O	5.570×10^{-2}	6.305×10^{-2}	5.660×10^{-2}	6.010×10^{-2}	6.305×10^{-2}
		FG-X	2.800×10^{-2}	3.124×10^{-2}	2.900×10^{-2}	3.140×10^{-2}	3.124×10^{-2}
	20	UD	2.520×10^{-2}	2.843×10^{-2}	2.580×10^{-2}	2.843×10^{-2}	2.843×10^{-2}
		FG-V	3.420×10^{-2}	3.880×10^{-2}	3.510×10^{-2}	3.780×10^{-2}	3.880×10^{-2}
		FG-O	4.510×10^{-2}	5.084×10^{-2}	4.580×10^{-2}	4.860×10^{-2}	5.084×10^{-2}
		FG-X	1.818×10^{-2}	2.058×10^{-2}	1.880×10^{-2}	2.040×10^{-2}	2.058×10^{-2}
	50	UD	2.230×10^{-2}	2.513×10^{-2}	2.280×10^{-2}	2.460×10^{-2}	2.513×10^{-2}
		FG-V	3.140×10^{-2}	3.570×10^{-2}	3.240×10^{-2}	3.480×10^{-2}	3.570×10^{-2}
		FG-O	4.200×10^{-2}	4.714×10^{-2}	4.860×10^{-2}	4.534×10^{-2}	4.714×10^{-2}
		FG-X	1.510×10^{-2}	1.729×10^{-2}	1.510×10^{-2}	1.720×10^{-2}	1.729×10^{-2}

0.14	10	UD	3.150×10^{-2}	3.530×10^{-2}	3.150×10^{-2}	3.470×10^{-2}	3.530×10^{-2}
		FG-V	3.867×10^{-2}	4.357×10^{-2}	3.867×10^{-2}	4.270×10^{-2}	4.357×10^{-2}
		FG-O	5.010×10^{-2}	5.663×10^{-2}	5.010×10^{-2}	5.370×10^{-2}	5.663×10^{-2}
		FG-X	2.566×10^{-2}	2.873×10^{-2}	2.566×10^{-2}	2.900×10^{-2}	2.873×10^{-2}
	20	UD	2.140×10^{-2}	2.430×10^{-2}	2.140×10^{-2}	2.370×10^{-2}	2.430×10^{-2}
		FG-V	2.900×10^{-2}	3.320×10^{-2}	2.900×10^{-2}	3.240×10^{-2}	3.320×10^{-2}
		FG-O	3.880×10^{-2}	4.395×10^{-2}	3.880×10^{-2}	4.190×10^{-2}	4.395×10^{-2}
		FG-X	1.555×10^{-2}	1.780×10^{-2}	1.555×10^{-2}	1.770×10^{-2}	1.780×10^{-2}
	50	UD	1.832×10^{-2}	2.090×10^{-2}	1.832×10^{-2}	2.050×10^{-2}	2.090×10^{-2}
		FG-V	2.610×10^{-2}	3.000×10^{-2}	2.610×10^{-2}	2.930×10^{-2}	3.000×10^{-2}
		FG-O	3.556×10^{-2}	4.010×10^{-2}	3.556×10^{-2}	3.840×10^{-2}	4.010×10^{-2}
		FG-X	1.245×10^{-2}	1.435×10^{-2}	1.245×10^{-2}	1.430×10^{-2}	1.435×10^{-2}
0.17	10	UD	3.536×10^{-2}	3.982×10^{-2}	3.536×10^{-2}	3.900×10^{-2}	3.982×10^{-2}
		FG-V	4.400×10^{-2}	5.011×10^{-2}	4.400×10^{-2}	4.890×10^{-2}	5.011×10^{-2}
		FG-O	5.810×10^{-2}	6.554×10^{-2}	5.810×10^{-2}	6.190×10^{-2}	6.554×10^{-2}
		FG-X	2.830×10^{-2}	3.214×10^{-2}	2.830×10^{-2}	3.230×10^{-2}	3.214×10^{-2}
	20	UD	2.547×10^{-2}	2.908×10^{-2}	2.547×10^{-2}	2.840×10^{-2}	2.908×10^{-2}
		FG-V	3.490×10^{-2}	4.015×10^{-2}	3.490×10^{-2}	3.910×10^{-2}	4.015×10^{-2}
		FG-O	4.762×10^{-2}	5.357×10^{-2}	4.762×10^{-2}	5.080×10^{-2}	5.357×10^{-2}
		FG-X	1.840×10^{-2}	2.116×10^{-2}	1.840×10^{-2}	2.110×10^{-2}	2.116×10^{-2}
	50	UD	2.248×10^{-2}	2.580×10^{-2}	2.248×10^{-2}	2.520×10^{-2}	2.580×10^{-2}
		FG-V	3.215×10^{-2}	3.710×10^{-2}	3.215×10^{-2}	3.620×10^{-2}	3.710×10^{-2}
		FG-O	4.440×10^{-2}	4.997×10^{-2}	4.440×10^{-2}	4.750×10^{-2}	4.997×10^{-2}
		FG-X	1.530×10^{-2}	1.774×10^{-2}	1.530×10^{-2}	1.770×10^{-2}	1.774×10^{-2}

Present[@]- Analytical non-polynomial shear deformation theory based on secant function.
Present[*]- Analytical non-polynomial shear deformation theory based on inverse hyperbolic sine function.
Present[$]- FE modeling using non-polynomial shear deformation theory based on secant function.
Present[&]- FE modeling using non-polynomial shear deformation theory based on inverse hyperbolic sine function.

The variation of the transverse shear stress (τ_{xz}) across the thickness of the simply supported carbon nanotube reinforced composite plate is Figure 4.4. The investigation is done through the application of analytical modelling of carbon nanotube reinforced composite plate within the context of non-polynomial shear deformation theory based on the secant function. The figure shows the variation of non-dimensional transverse shear stresses with normalized thickness for different distribution of the carbon nanotubes. Here, the simply supported square carbon nanotube reinforced composite plate subjected to the sinusoidal loading condition with span thickness ratio of 50 is

considered for the analysis. It is observed from the figure that for a particular value of span thickness ratio and volume fraction of the CNTs, the non-dimensional transverse shear stress is maximum for FG-O distribution and minimum for FG-X distribution. It is also observed from the figure that for the symmetrical distribution i.e. FG-O, FG-X, and UD of the CNTs in the composite plate, the distribution of the non-dimensional transverse shear stresses are also symmetrical along the central axis. From the figure, it is observed that the transverse shear stresses at the top and bottom of the carbon nanotubes reinforced composite plate is insignificant which establishes the traction free condition at the top and bottom of the plate.

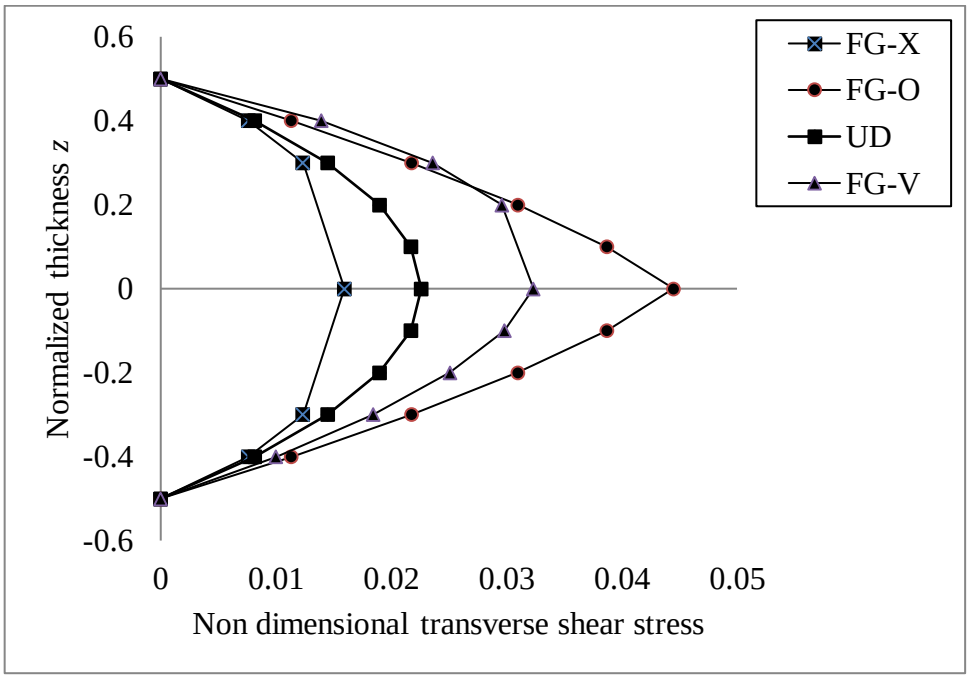

Figure 4.4. Variation of non-dimensional transverse shear stresses (τ_{xz}) with normalized thickness

4.2.2. Free Vibration analysis of carbon nanotube reinforced composite plate

The vibration analysis is an essential tool used to evaluate the condition of structures. It is used to identify the root causes of problems, detect faults, and prevent failures. Vibration analysis is a critical aspect of structural analysis, and it involves the measurement, analysis, and interpretation of the vibration signals generated by structures. There are two types of vibration analysis: free vibration analysis and forced

vibration analysis. Free vibration analysis is a technique used to analyze the natural frequencies and mode shapes of a structure. It involves exciting the structure and then letting it vibrate freely, without any external forcing. This type of analysis is crucial in determining the dynamic characteristics of a structure and can be used to predict its behaviour under different operating conditions. The importance of free vibration analysis in structure cannot be overstated. It is a critical tool used to evaluate the structural integrity of system and to identify any potential problems before they lead to failure. Free vibration analysis is used in a wide range of applications, including the evaluation of turbine blades, pump impellers, and other critical components. One of the primary benefits of free vibration analysis is that it allows engineers to determine the natural frequencies of a structure. These natural frequencies are the frequencies at which the structure will vibrate when excited. By understanding the natural frequencies of a structure, engineers can design equipment to avoid these frequencies and prevent resonant vibrations, which can cause damage to the equipment. Another benefit of free vibration analysis is that it allows engineers to identify the mode shapes of a structure. Mode shapes are the patterns of vibration that occur when a structure is excited at its natural frequencies. By understanding the mode shapes of a structure, engineers can design the structure to avoid these modes and prevent damage to the structure. Free vibration analysis can also be used to diagnose problems in structures. By analyzing the vibration signals generated by a structure, engineers can identify the root cause of any problems and take corrective action before a failure occurs. Free vibration analysis is also a valuable tool for predicting the behaviour of structures under different operating conditions. By understanding the natural frequencies and mode shapes of a structure, engineers can predict how it will behave when subjected to different loads when operated. This information is crucial in designing of structure that can operate safely

and reliably under a wide range of operating conditions. In addition to its application in structural maintenance, free vibration analysis is also used in other fields, such as aerospace and automotive engineering. In aerospace engineering, free vibration analysis is used to evaluate the structural integrity of aircraft and spacecraft. In automotive engineering, it is used to evaluate the durability of car components, such as suspension systems and engine mounts.

The free vibration analysis of the carbon nanotube reinforced composite plates includes the natural frequencies and the higher modes of vibration of the plates due to the variation of the different parametric conditions which mainly incorporates the variation of the reinforcement distribution pattern of carbon nanotubes across the thickness of the carbon nanotube reinforced composite plate, volume fraction of carbon nanotubes in carbon nanotube reinforced composite plate, and side to thickness ratio.

To validate the FE modeling, the convergence of the FE solutions for non-dimensional natural frequency is presented in Figure 4.5. For the convergence study of the FE solutions, FG-X reinforcement distributed carbon nanotube reinforced composite plate with the volume fraction of 0.11 and span thickness ratio of 10 is selected for the analysis. For this analysis, the non-polynomial shear deformation theory based on secant function is adopted. The convergence study is obtained for different mesh sizes varying from 2x2 to 16x16 and is plotted. It is observed from the figure that the results of normalized natural frequency have converged at a mesh size of 8x8, i.e., 64 numbers of elements. Hence, if not specified further, all the results are obtained at the mesh size of 8x8.

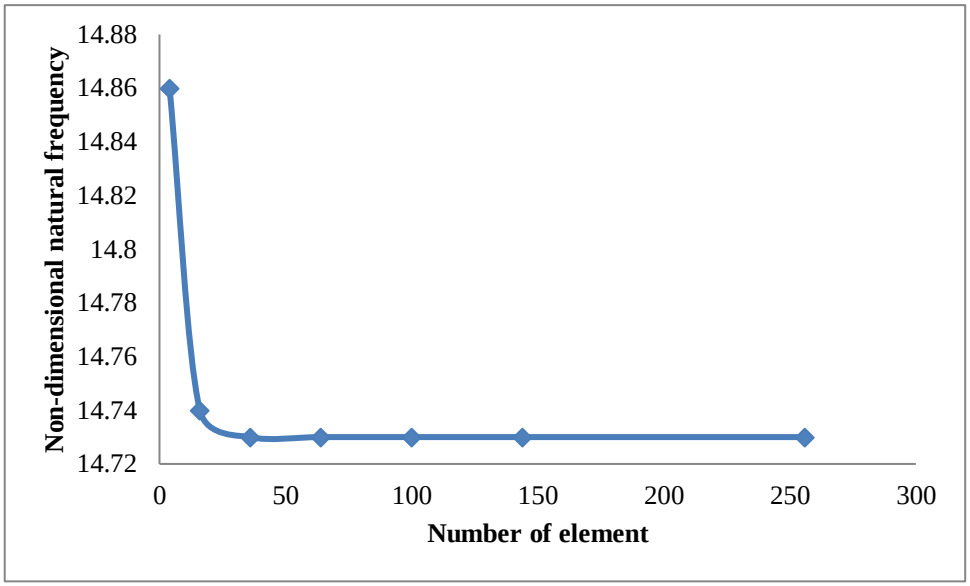

Figure 4.5. Convergence of the FE solutions for non-dimensional natural frequency

Further, the non-dimensional fundamental frequency is computed for carbon nanotube reinforced composite plate for different span thickness ratio, CNTs distribution and volume fraction of CNTs is discussed in detail. Here, simply supported square carbon nanotube reinforced composite plates with different distributed pattern of carbon nanotubes across the thickness direction are considered. The presented results for non-dimensional natural frequency of carbon nanotube reinforced composite plate are based on analytical and FE method within the context of non-polynomial shear deformation theory based on the secant function and inverse hyperbolic sine function. Non-dimensional parameter used for the representation of the results is given in sub section 3.11. The provided results demonstrate good agreement when these are compared with the FSDT and ANSYS results of Zhu et al. (2012). It is observed from the Table 4.6 that in case of a particular span thickness ratio and volume fraction of the CNTs, non-dimensional natural frequency is minimum for FG-O and maximum for FG-X. It is observed form the table that for a particular volume fraction of CNTs, the non-dimensional natural frequency increases with an increase in the span thickness ratios for all types of CNTs distributions. Similarly, for a particular span thickness ratio, non-

dimensional natural frequency increases with increase in the volume fraction of CNTs for all types of the CNTs distribution.

Table 4.6: Non dimensional natural frequency of simply supported CNTRC plate

Distribution	V^*_{CNT}	b/h	Present[@]	Present[*]	Present[$]	Present[&]	Zhu et al. (2012)[#]	Zhu et al. (2012)[^]
UD	0.11	10	13.6875	13.0459	13.5517	13.5897	13.5320	13.5210
		20	17.3698	17.3348	17.3138	17.3307	17.3550	17.3280
		50	19.2000	19.1639	19.1595	19.1630	19.2230	19.1840
	0.14	10	14.5150	13.7232	14.3559	14.4021	14.3060	14.2960
		20	18.9800	18.9293	18.9079	18.9899	18.9210	18.8930
		50	21.3000	21.3295	21.3222	21.3269	21.3540	21.3110
	0.17	10	16.9994	16.2244	16.8334	16.8796	16.8150	16.8010
		20	21.4673	21.4263	21.4002	21.4204	21.4560	21.4220
		50	23.6000	23.6181	23.6132	23.6173	23.6970	23.6490
FG-V	0.11	10	12.4650	12.2399	12.4568	12.4850	12.4520	12.4950
		20	15.1300	15.1026	15.0734	15.0839	15.1100	15.1030
		50	16.2690	16.2023	16.2046	16.2065	16.2520	16.2160
	0.14	10	13.3240	12.9736	13.3118	13.3158	13.2560	13.3000
		20	16.6310	16.5287	16.5130	16.5077	16.5100	16.5030
		50	18.0010	17.9721	17.9828	17.9761	17.9950	17.9560
	0.17	10	15.4720	15.1968	15.4497	15.4830	15.4610	15.5140
		20	18.8240	18.6167	18.5857	18.5978	18.6380	18.6280
		50	20.0240	19.9170	19.9232	19.9254	19.9820	19.9380
FG-O	0.11	10	11.5620	11.0690	11.3208	11.3130	11.5500	11.6000
		20	13.5410	13.3757	13.3970	13.3897	13.5230	13.5310
		50	14.3160	14.2364	14.2493	14.2477	14.3020	14.2900
	0.14	10	12.3410	11.7941	12.1140	12.1125	12.3380	12.3910
		20	14.7920	14.6400	14.6649	14.6587	14.7840	14.7940
		50	15.8520	15.7540	15.7684	15.7668	15.8010	15.7880
	0.17	10	14.2930	13.8116	14.0822	14.0849	14.2820	14.3450
		20	16.6490	16.4920	16.5156	16.5130	16.6280	16.6400
		50	17.6260	17.4721	17.4917	17.4910	17.5440	17.5290
FG-X	0.11	10	14.6240	13.8874	14.6754	14.7330	14.6160	14.6590
		20	19.6420	19.9580	19.9093	19.9440	19.9390	19.9160
		50	23.0000	22.9272	22.9036	22.9118	22.9840	22.9100
	0.14	10	15.3740	14.4260	15.3963	15.4595	15.3680	15.4130
		20	21.6570	21.6258	21.5970	21.6366	21.6420	21.6200
		50	25.5610	25.5281	25.4997	25.5097	25.5550	25.4740
	0.17	10	18.3610	17.1378	18.1770	18.2379	18.2780	18.3300
		20	24.7820	24.6289	24.6031	24.6364	24.7640	24.7350
		50	28.5310	28.2966	28.2724	28.2800	28.4130	28.3220

Present[@]- Analytical non-polynomial shear deformation theory based on secant function.
Present[*]- Analytical non-polynomial shear deformation theory based on inverse hyperbolic sine function.
Present[$]- FE modeling using non-polynomial shear deformation theory based on secant function.
Present[&]- FE modeling using non-polynomial shear deformation theory based on inverse hyperbolic sine function. [#]FSDT, and [^] ANSYS

In free vibration analysis, understanding the reaction of a structure after being subjected to an initial disturbance and allowed to vibrate freely depends critically on

mode shapes. The spatial distribution of the structure's displacements and deformations at various frequencies are represented by mode shapes. Each mode shape represents a certain natural frequency of vibration and reveals the major directions and magnitudes in which a structure reacts. Engineers can spot resonance, which happens when the stimulation frequency coincides with the natural frequency and results in excessive vibrations and probable structural collapse, by analysing mode forms. If resonance is not adequately managed, it can be dangerous, leading to wear and tear, and even disastrous results. In order to identify the key modes and reduce the hazards related to resonance events, mode shape analysis is crucial.

Further, figure 4.6 shows the first six free vibration mode shapes of simply supported square carbon nanotube reinforced composite plate as discussed in the earlier problem, considering the span thickness ratio to be 50. The investigation is done through the application of analytical modelling of carbon nanotube reinforced composite plate using non-polynomial shear deformation theory based on the secant function. It is observed from the figure that the eigen values corresponding to modes (m = 2, n = 1) and (m = 2, n = 2) are of higher order over (m = 1, n = 3) and (m = 1, n = 4) due to difference in the mechanical property in the longitudinal and transverse directions.

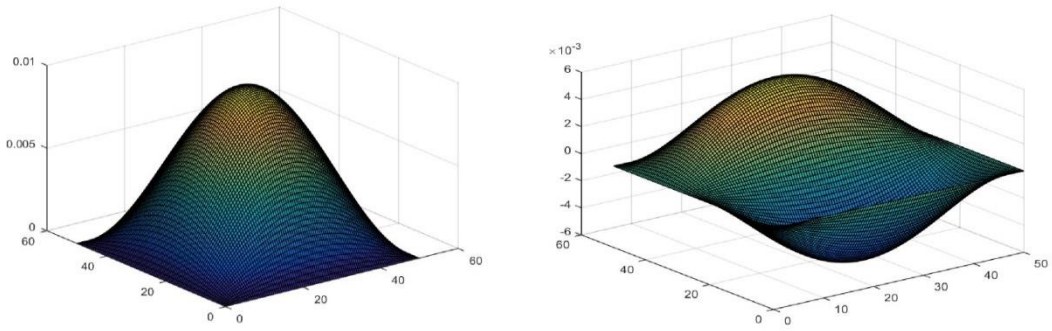

(a) (b)

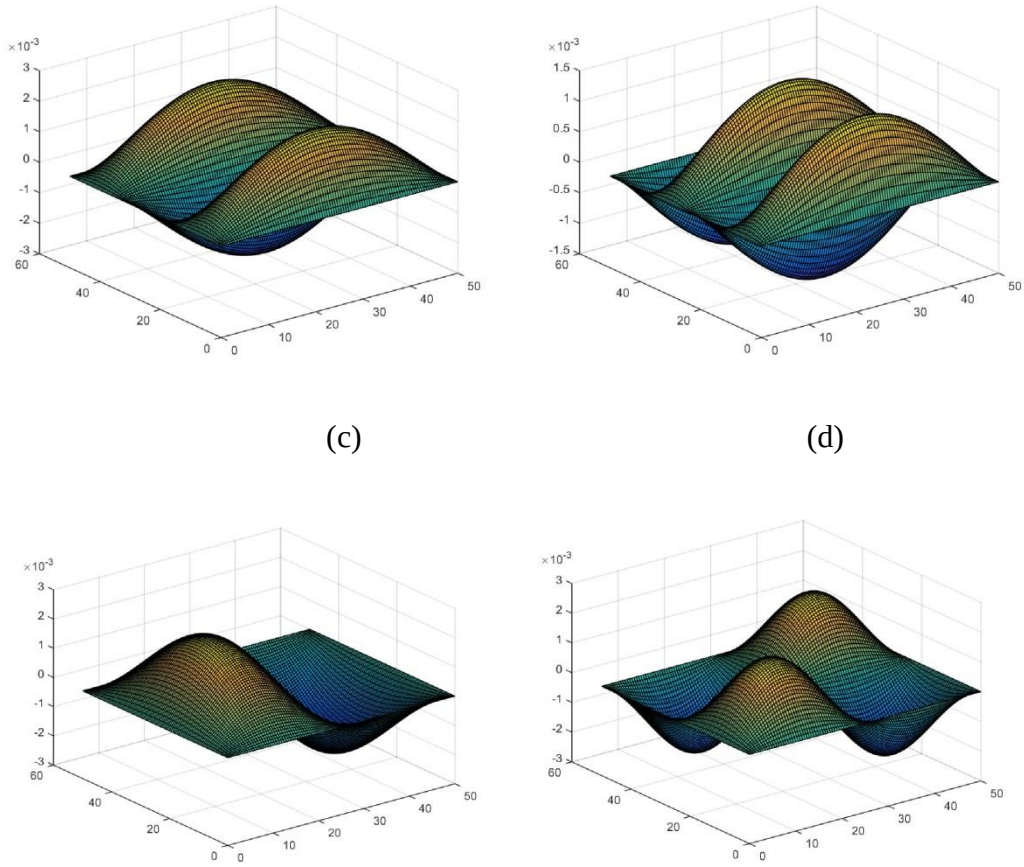

Figure 4.6. Free vibration mode shape of CNTRC plate. (a) 1st Mode (m = 1, n = 1); (b) 2nd Mode (m = 1, n = 2); (c) 3rd Mode (m = 1, n = 3); (d) 4th Mode (m = 1, n = 4); (e) 5th Mode (m = 2, n = 1); (f) 6th Mode (m = 2, n = 2)

4.2.3. Buckling analysis of carbon nanotube reinforced composite plate

In this section, the buckling analysis of the carbon nanotube reinforced composite plate under uniaxial compressive load and biaxial compressive load is carried out in detail. Buckling is a phenomenon that occurs when a structure, such as a column, beam, and plates is subjected to an axial load. When the load exceeds a critical value, the structure will fail due to instability, rather than the load itself. Buckling is a complex phenomenon that is influenced by many factors, including the material properties of the structure, its geometry, and the load applied. Buckling load analysis is an essential tool used in structural maintenance to evaluate the strength and stability of structures. The importance of buckling load analysis in structures maintenance cannot be overstated. It

is a critical tool used to evaluate the structural integrity of structures and to identify any potential problems before they lead to failure. Buckling load analysis is used in a wide range of applications, including the evaluation of columns, beams, plate and other critical components. One of the primary benefits of buckling load analysis is that it allows engineers to determine the critical buckling load of a structure. The critical buckling load is the load at which the structure will buckle or fail due to instability. By understanding the critical buckling load of a structure, engineers can design structures to avoid this load and prevent buckling, which can cause damage to the structures. Another benefit of buckling load analysis is that it allows engineers to evaluate the strength of a structure under different loading conditions. By analyzing the buckling load of a structure under different loads, engineers can design structures that can operate safely and reliably under a wide range of operating conditions. Buckling load analysis can also be used to diagnose problems in structures. By analyzing the buckling behavior of a structure, engineers can identify the root cause of any problems and take corrective action before a failure occurs. For example, if a column is buckling due to inadequate bracing, engineers can design additional bracing to prevent further buckling. Buckling load analysis is also a valuable tool for predicting the behavior of structures under different operating conditions. By understanding the critical buckling load of a structure, engineers can predict how it will behave when subjected to different loads or when operating at different temperatures or pressures. This information is crucial in designing structures that can operate safely and reliably under a wide range of operating conditions. The critical buckling load for the carbon nanotube reinforced composite plates includes buckling analysis due to uniaxial and biaxial loading. The detailed buckling response of the carbon nanotube reinforced composite plates is explored due to the variation of the different parametric conditions which mainly incorporates the

variation of the reinforcement distribution pattern of carbon nanotubes across the thickness of the carbon nanotube reinforced composite plate, volume fraction of carbon nanotubes in carbon nanotube reinforced composite plate, and side to thickness ratio.

To validate the FE modeling, the convergence of the FE solutions for non-dimensional critical buckling loads subjected to uniaxial compression load is presented in Figure 4.7. For the convergence study of the FE solutions, the non-polynomial shear deformation theory based on inverse hyperbolic sine function is adopted. The FG-X reinforcement distributed carbon nanotube reinforced composite plate with the volume fraction of carbon nanotube as 0.11 with different span thickness ratios are selected for the analysis. The non-dimensional buckling load is obtained for different mesh sizes varies from 2x2 to 16x16 and is plotted. It is observed from the figure that the normalized critical buckling loads are converged at a mesh size of 8x8, i.e., 64 numbers of elements. Hence, if not specified further, all the results are obtained at the mesh size of 8x8.

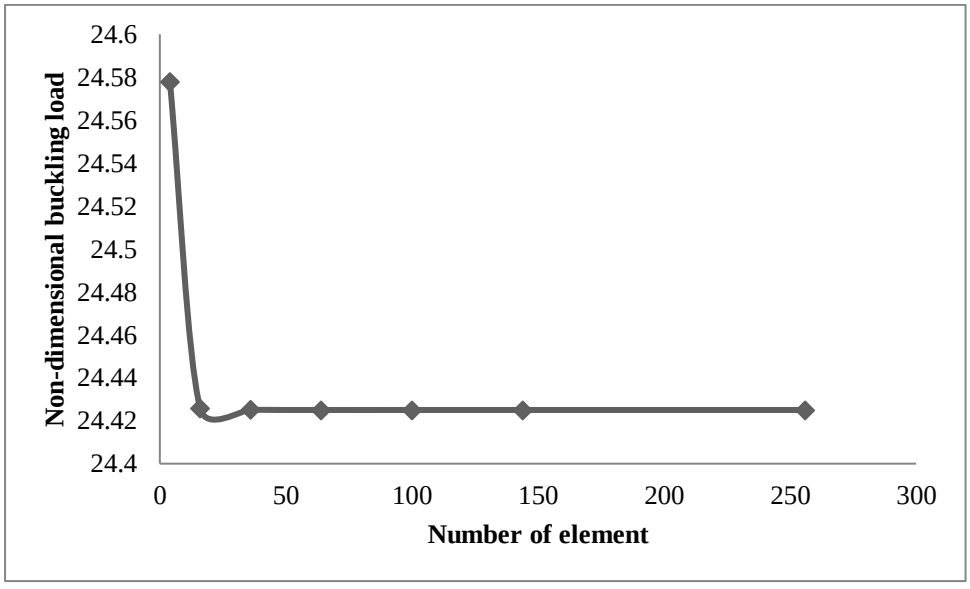

Figure 4.7. Convergence of the FE solutions for non-dimensional critical buckling load (S=10)

4.2.3.1. Buckling analysis of the carbon nanotube reinforced composite plate under uni-axial compressive load

The non-dimensional buckling load analysis of simply supported CNTRC plate subjected to the uniaxial compressive load (Ψ_x= -1, Ψ_y= 0) is obtained in Table 4.7. Here are the findings for the non-dimensional buckling load of a carbon nanotube reinforced composite plate under uniaxial compressive load. The analytical and FE results for non-dimensional buckling loads of carbon nanotube reinforced composite plate are obtained using non-polynomial shear deformation theories based on the secant function and inverse hyperbolic sine function. For the analysis of non-dimensional buckling load of the simply supported carbon nanotube reinforced composite plate, different distribution of carbon nanotube reinforcement pattern is selected from Table 3.1. The material property selected here, is given in Table 3.3 and the non-dimensional parameter selected from sub section 3.11. The analysis is conducted for UD symmetrical reinforcement distribution pattern of CNTs across the thickness of the CNTRC plate. The effect of different parametric condition i.e., volume fraction of CNTs in CNTRC plate, and side to thickness ratio on the non-dimensional buckling is also presented. The presented results for non-dimensional critical buckling load under uniaxial compressive load are compared with the results of Wattanasakulpong and Chaikittiratana (2015). It is observed from the table that the present results are closely agreed with the established results. From the table it is also observed that, the non-dimensional critical buckling load under uniaxial compressive load of CNTRC plate increases as the value of volume fraction of CNTs in CNTRC plate increases. Further, it is observed that, for unsymmetrical FG-V distribution, the non-dimensional critical buckling load under uniaxial compressive load of CNTRC plate increases as the value of volume fraction of CNTs in CNTRC plate increases. The FG-O reinforcement distribution pattern of CNTs across the thickness of the CNTRC plate produces the lowest resistance non-dimensional critical buckling load under uniaxial compressive

load which can simply be observed. Also, it is observed that the FG-X reinforcement distribution pattern of CNTs across the thickness of the CNTRC plate produces the maximum resistance to the non-dimensional critical buckling load under uniaxial compressive load.

Table 4.7: Non dimensional critical buckling load under uniaxial compressive load for simply supported square CNTRC plates

Distribution	V^*_{CNT}	***b/h***	**Present[@]**	**Present[*]**	**Present[$]**	**Present[&]**	**[Ref (2015)]^**	**[Ref (2015)]#**
UD	0.11	10	20.6812	21.0820	20.6777	20.7947	20.6814	20.7286
		20	33.5331	33.7323	33.5480	33.6137	-	-
		50	40.9515	40.9943	40.9752	40.9898	-	-
	0.14	10	23.3556	23.8919	23.3450	23.4964	23.3559	23.4229
		20	40.2436	40.5310	40.2606	40.3544	-	-
		50	51.0410	51.1062	51.0707	51.0930	-	-
	0.17	10	32.3177	32.9265	32.3136	32.4921	32.3180	32.3890
		20	51.8832	52.1821	51.9068	52.0054	-	-
		50	62.9948	63.0585	63.0315	63.0533	-	-
FG-V	0.11	10	17.4915	17.7617	17.4988	17.5789	-	-
		20	25.4214	25.5286	25.4449	25.4806	-	-
		50	29.2838	29.3043	29.3140	29.3212	-	-
	0.14	10	20.0012	20.3687	20.0063	20.1124	-	-
		20	30.6284	30.782	30.6568	30.7080	-	-
		50	36.2545	36.2847	36.2927	36.3033	-	-
	0.17	10	27.2407	27.6324	27.2617	27.3805	-	-
		20	39.1299	39.2809	39.1769	39.2282	-	-
		50	44.8172	44.8456	44.8759	44.8860	-	-
FG-O	0.11	10	14.4994	14.4132	14.4497	14.4307	14.4990	14.4515
		20	20.1048	20.0412	20.0917	20.0699	-	-
		50	22.6379	22.6236	22.6643	22.6590	-	-
	0.14	10	16.6988	16.6223	16.6450	16.6419	16.6984	16.6451
		20	24.2442	24.1697	24.2261	24.2059	-	-
		50	27.8983	27.8803	27.9310	27.9254	-	-
	0.17	10	22.6828	22.6197	22.6469	22.6569	22.6823	22.6276
		20	30.9079	30.8514	30.9237	30.9144	-	-
		50	34.5229	34.5100	34.5869	34.5842	-	-
FG-X	0.11	10	24.2858	25.0167	24.2338	24.4250	24.2864	24.3943
		20	44.3635	44.8623	44.35101	44.5043	-	-
		50	58.5467	58.6759	58.55425	58.5961	-	-
	0.14	10	26.8934	27.7528	26.8367	27.0581	26.8941	27.0177
		20	52.5263	53.1503	52.5149	52.7086	-	-
		50	73.0335	73.2073	73.0421	73.0996	-	-
	0.17	10	37.6932	38.6099	37.6522	37.9059	37.6944	38.8069
		20	68.6105	69.1926	68.5925	68.7791	-	-
		50	90.3692	90.5155	90.3594	90.4086	-	-

Present[@]- Analytical non-polynomial shear deformation theory based on secant function.
Present[*]- Analytical non-polynomial shear deformation theory based on inverse hyperbolic sine function.

Present[$]- FE modeling using non-polynomial shear deformation theory based on secant function. Present[&]- FE modeling using non-polynomial shear deformation theory based on inverse hyperbolic sine function. [Ref (2015)] - Wattanasakulpong and Chaikittiratana (2015). [^]TSDT, [#]SSDT

Further, the effect of side to thickness ratio on the non-dimensional critical buckling load under uni-axial loading (Ψ_x= -1, Ψ_y= 0) condition of CNTRC plate is shown in the Figure 4.8. The investigation is done through the application of analytical modelling of carbon nanotube reinforced composite plate within the context of non-polynomial shear deformation theory based on the inverse hyperbolic sine function. Different CNTs reinforcement distribution pattern with the volume fraction of 0.11 is considered for the analysis. Non-dimensional critical buckling load of all symmetrical reinforcement distribution pattern (UD, FG-X, and FG-O) of CNTs under uniaxial loading (Ψ_x= -1, Ψ_y= 0) condition across the thickness of the CNTRC plate are obtained. It is observed from the table that the non-dimensional critical buckling load under uniaxial loading condition increases as the value of the side to thickness ratio increases. For smaller side to thickness ratio, the rate of increase in the non-dimensional critical buckling load under uniaxial loading condition is maximum as compared to the higher side to thickness ratio. As the side to thickness ratio increases to infinity the rate of change in the increase in the non-dimensional critical buckling load under uni-axial loading condition approaches to zero.

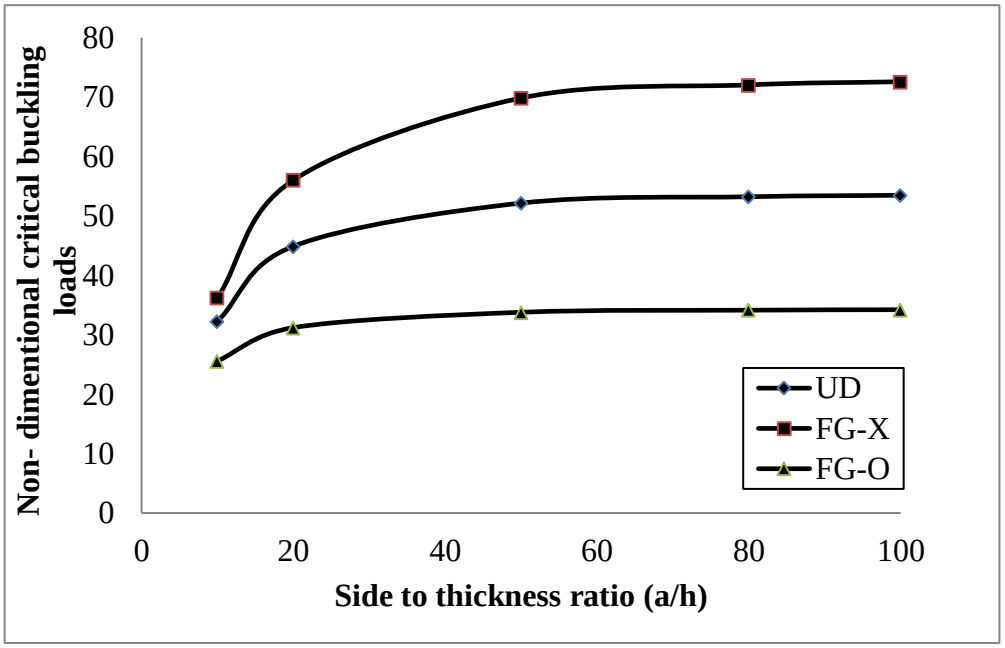

Figure 4.8. The effect of variation of side to thickness ratio on non-dimensional critical buckling load under uni-axial loading (Ψ_x= -1, Ψ_y= 0) condition

4.2.3.2. Buckling analysis of the carbon nanotube reinforced composite plate under bi-axial compressive load

The non-dimensional buckling analysis of simply supported CNTRC plate subjected to the bi-axial compressive load (Ψ_x= -1, Ψ_y= -1) is mentioned in tabular format for different distributed pattern of carbon nanotube in CNTRC plate. The analysis is conducted for different symmetrical reinforcement distribution pattern of CNTs across the thickness of the CNTRC plate, volume fraction of CNTs in CNTRC plate and side to thickness ratios. For the analysis of non-dimensional buckling load of the simply supported carbon nanotube reinforced composite plate, different distribution of carbon nanotube reinforcement pattern is selected from Table 3.1. The material property selected here, is given in Table 3.3 and the non-dimensional parameter selected from sub section 3.11. Here are the findings for the non-dimensional buckling load for carbon nanotube reinforced composite plate under a biaxial compressive load. These are derived using analytical and FE method using the non-polynomial shear deformation

theories based on the secant function and inverse hyperbolic sine function. The presented results for non-dimensional critical buckling load under biaxial compressive load are compared with the results of Wattanasakulpong and Chaikittiratana (2015) and it is observed that the present results are closely agreed with the published results of Wattanasakulpong and Chaikittiratana (2015). From the Table 4.8**,** it is also observed that, non-dimensional critical buckling load under biaxial compressive load for uniformly distributed CNTRC plate increases as the value of volume fraction of CNTs in CNTRC plate increases. Similarly, it is observed that, the non-dimensional critical buckling load under biaxial compressive load for FG-V distributed CNTRC plate increases as the value of volume fraction of CNTs in CNTRC plate increases. The FG-O reinforcement distribution pattern of CNTs across the thickness of the CNTRC plate produces the lowest resistance to non-dimensional critical buckling load under biaxial compressive load which can be simply observed. Also, it is seen that the FG-X reinforcement distribution pattern of CNTs across the thickness of the CNTRC plate produces the highest resistance to the non-dimensional critical buckling load under biaxial compressive load.

Table 4.8: Non dimensional critical buckling load under bi-axial compressive load for simply supported square CNTRC plates

Distribution	V^*_{CNT}	***b/h***	**Present[@]**	**Present[*]**	**Present[$]**	**Present[&]**	**Ref (2015)**	**Ref (2015)**
UD	0.11	10	10.3406	10.5410	10.3406	10.5410	10.3407	10.3643
		20	16.7665	16.8661	16.7665	16.8661	-	-
		50	20.4757	20.4972	20.4757	20.4972	-	-
	0.14	10	11.6778	11.9460	11.6778	11.9460	11.6770	11.7115
		20	20.1218	20.2655	20.1218	20.2655	-	-
		50	25.5205	25.5531	25.5205	25.5531	-	-
	0.17	10	16.1588	16.4633	16.1588	16.4633	16.1590	16.1945
		20	25.9416	26.0911	25.9416	26.0911	-	-
		50	31.4974	31.5293	31.4974	31.5293	-	-
FG-V	0.11	10	8.7457	8.8809	8.7457	8.8809	-	-
		20	12.7107	12.7643	12.7107	12.7643	-	-
		50	14.6419	14.6522	14.6419	14.6522	-	-
	0.14	10	10.0006	10.1844	10.0006	10.1844	-	-
		20	15.3142	15.3910	15.3142	15.3910	-	-
		50	18.1273	18.1424	18.1273	18.1424	-	-

	0.17	10	13.6203	13.8162	13.6203	13.8162	-	-
		20	19.5649	19.6405	19.5649	19.6405	-	-
		50	22.4086	22.4228	22.4086	22.4228	-	-
	0.11	10	7.2497	7.2066	7.2497	7.2066	7.2495	7.2257
		20	10.0524	10.0206	10.0524	10.0206	-	-
		50	11.3189	11.3118	11.3189	11.3118	-	-
FG-O	0.14	10	8.3494	8.3112	8.3494	8.3112	8.3492	8.3225
		20	12.1221	12.0849	12.1221	12.0849	-	-
		50	13.9491	13.9401	13.9491	13.9401	-	-
	0.17	10	11.3414	11.3098	11.3414	11.3098	11.3412	11.3138
		20	15.4540	15.4257	15.4540	15.4257	-	-
		50	17.2615	17.2550	17.2615	17.2550	-	-
	0.11	10	12.1429	12.5084	12.1429	12.5084	12.1432	12.1972
		20	22.1817	22.4312	22.1817	22.4312	-	-
		50	29.2733	29.3379	29.2733	29.3379	-	-
FG-X	0.14	10	13.4467	13.8764	13.4467	13.8764	13.4471	13.5089
		20	26.2631	26.5751	26.2631	26.5751	-	-
		50	36.5167	36.6037	36.5167	36.6037	-	-
	0.17	10	18.8469	19.3050	18.8469	19.3050	18.8472	18.9035
		20	34.3053	34.5963	34.3053	34.5963	-	-
		50	45.1846	45.2577	45.1846	45.2577	-	-

Present[@]- Analytical non-polynomial shear deformation theory based on secant function.
Present[*]- Analytical non-polynomial shear deformation theory based on inverse hyperbolic sine function.
Present[$]- FE modeling using non-polynomial shear deformation theory based on secant function.
Present[&]- FE modeling using non-polynomial shear deformation theory based on inverse hyperbolic sine function. [Ref (2015)] Wattanasakulpong and Chaikittiratana (2015)

Further, the mode shape analysis is essential for buckling load analysis, which assesses a structure's stability under compressive loads. When a thin structure, such a column or beam, collapses from instability under compressive stresses, buckling takes place. In order to maintain structural integrity and avoid catastrophic failures, it is essential to understand the critical buckling loads. Mode shapes aid in identifying a structure's buckling modes and associated buckling stresses. Engineers can determine the weakest places in the structure and gauge its susceptibility to buckling by analysing these mode forms. This knowledge is crucial for creating structures that can sustain expected loads and retain stability for the course of their useful lives.

In Figure 4.9, the buckling mode shapes for the pervious problem are drawn for the FG-X reinforcement distribution pattern of CNTs across the thickness of the simply supported CNTRC plate with side to thickness ratio of 10 and volume fraction of CNTs of 0.17. The investigation is done through the application of analytical modelling of

carbon nanotube reinforced composite plate using the secant function based non-polynomial shear deformation theory.

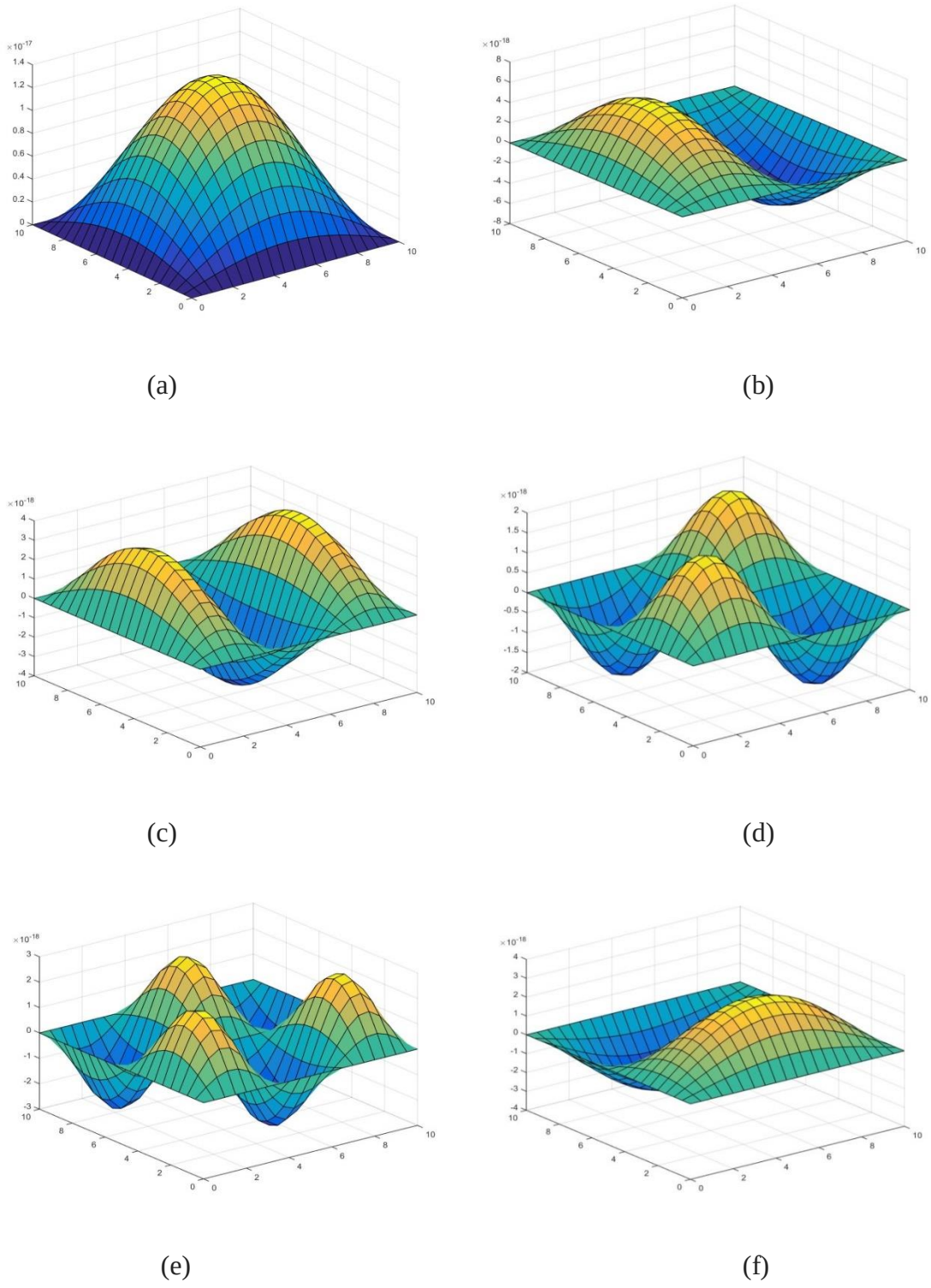

Figure 4.9. First six buckling mode shapes carbon nanotube reinforced composite plate

4.3. Structural analysis of the carbon nanotube reinforced sandwich plate

After deriving the bending, free vibration, and buckling responses of carbon nanotube reinforced composite plate, the structural responses of carbon nanotube reinforced sandwich plates are investigated.

Sandwich plates have thin face sheets made up of carbon nanotube reinforced composite plate and thick core layers made up of weak materials in comparison to the materials of the face sheets. Such a configuration facilitates weight reduction. In this example, two face sheets are considered at the top and bottom of the sandwich plate with different core to face sheet thickness ratios. In this section, the static and free vibration analysis of functionally graded carbon nano-tubes reinforced (FG-CNTR) sandwich plates are studied in the framework of non-polynomial shear deformation theories based on secant function and inverse hyperbolic sine function. The governing differential equations are derived using Hamilton's principle and solved with the Navier's solution technique and FE modelling. The analytical and FE approaches are used to obtain the deflections, stresses, natural frequencies, and corresponding mode shapes of FG-CNTR sandwich plates with different material properties, stacking sequences, span thickness ratios, core to face sheet thickness ratios, and loading conditions. Different types of reinforcement distribution such as uniformly distribution (UD) and functionally graded (FG) distribution of FG-O, FG-X, FG-/\, and FG-V are considered for the analysis. Also, the effort is made to achieve the best possible arrangement for the stacking sequences and the appropriate reinforcement distribution that will produce improved static and free vibration responses for the FG-CNTR sandwich plates.

The FG-CNTR sandwich plate is of three layers, the top face sheet is ($Z_0 - Z_1$) i.e. h_f and the bottom face sheet is ($Z_3 - Z_2$) and a core ($Z_1 - Z_2$) i.e. h_c. The detailed coordinate

axes with depth of different layers are shown in Figure 4.10. Four different types of models are considered here for the analyses which are as follows:

a) UD CNTRC plate is used as the face sheet along with the homogenous core.
b) FG CNTRC plate is used as the face sheet along with the homogenous core.
c) The homogenous plate is used as the face sheet along with the UD CNTRC plate used as core.
d) The homogenous plate is used as the face sheet along with the FG CNTRC plate used as core.

The models (a) and (b) is show in Figure 4.11 represent FG-O distributed carbon nanotube reinforced composite plate as face sheet with homogenous core and homogenous face sheet with FG-O distributed core.

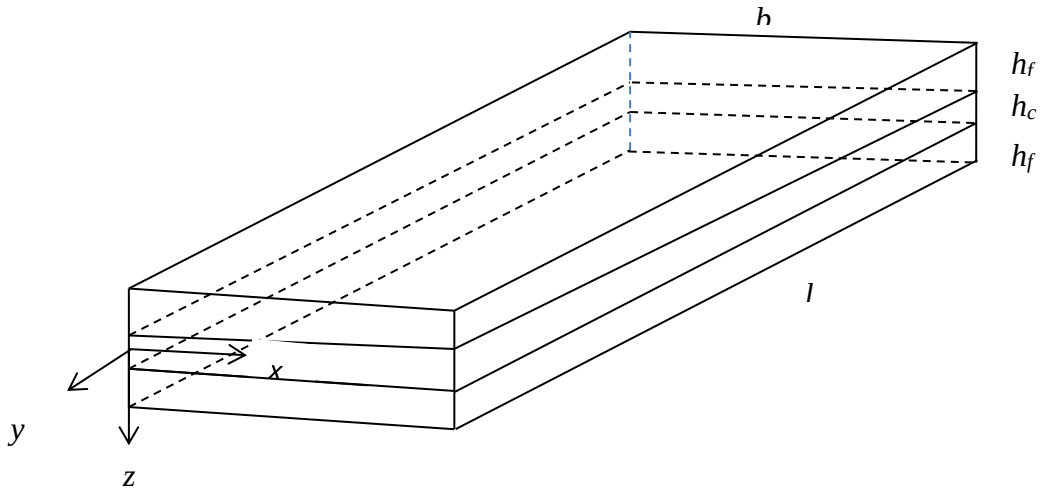

(a)

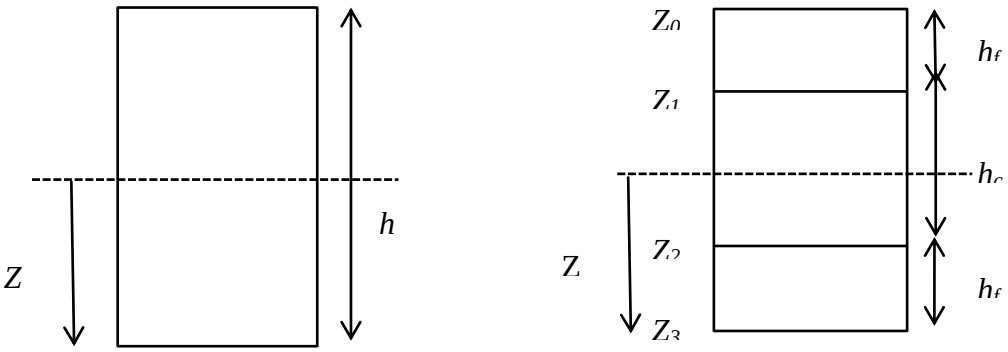

Figure 4.10. Coordinate system of a rectangular plate (a) *x* and *y* are in plane and *z* is along the thickness direction: (b) CNTRC plate cross section: (c) FG-CNTR sandwich plate of three layer in which h_f is the face sheet thickness h_c is the core thickness

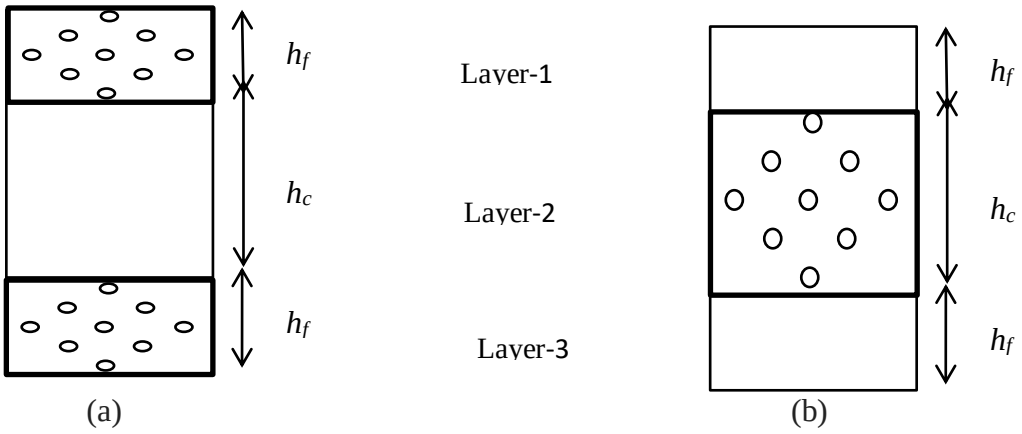

Figure 4.11. (a) Three layered sandwich plate with layer-1 and layer-3 is FG-CNTR plate and layer-2 is homogenous layer. (b) Layer-1 and layer-3 is homogenous layer and layer-2 is FG-CNTR plate

4.3.1. Bending analysis of the carbon nanotube reinforced sandwich plate

In this section different numerical problem, based on bending analysis of the FG-CNTR sandwich plates are solved for different material properties, stacking sequences, span thickness ratios, core to face sheet thickness ratios, and loading conditions. This section is further divided into three sub sections in which the results for non-dimensional transverse and in plane deflection, normal stresses and transverses shear stresses are discussed in detail. The results for every analysis consist of analytical results followed by the FE results using non-polynomial shear deformation theories based on the secant function and inverse hyperbolic sine function.

4.3.1.1. Transverse and in plane deflection of the carbon nanotube reinforced sandwich plate

In this section, the simply supported carbon nanotube reinforced sandwich plate subjected to sinusoidal loading condition is analyzed for transverse deflection and in

plane deflections. Different stacking sequences for the analysis are selected and the effort is made to achieve the best stacking sequence.

The non-dimensional in plane and transverse displacements for different span thickness ratios, core to face thickness ratios and volume fractions of CNTs for a simply supported square FG-CNTR sandwich plate is presented in Table 4.9 (a) and Table 4.9 (b), respectively. The results for non-dimensional transverse and in plane deflection of a carbon nanotube reinforced sandwich plate under sinusoidal load are shown here. The results are obtained using the analytical and FE method within the framework of non-polynomial shear deformation theories based on the secant function and inverse hyperbolic sine function. Here, L1 stacking sequences are considered for the analyses. For the analysis of non-dimensional transverse deflection of the simply supported carbon nanotube reinforced composite plate different stacking sequence selected from Table 3.6. The material property selected here, is given in Table 3.3 and the non-dimensional parameter selected from sub section 3.11. In CNTRC plate PMMA is used as the matrix along with the CNTs fibers. FG-T and FG-B distributions are considered as the top and bottom face sheet respectively which are mentioned in table 3.2. Titanium alloy (T) is used as the homogenous core in the FG-CNTR sandwich plate. The obtained results are compared with the results published by Natarajan *et al.* (2014) using different shear deformation theory with 13 degrees of freedom. The present theory involves with five unknown kinematic variables that make it efficient for computation prospective. It is observed from the table that the present results show well agreement with the existing results. It can also be observed from the table that, for a particular span thickness ratio and core to face sheet thickness ratio the non-dimensional in-plane displacements and transverse displacements reduce as the volume fraction of the CNTs are increasing whereas the value of transverse displacements is decreasing and in-plane

displacements are increasing with the increase in the span thickness ratios. For a particular span thickness ratio and volume fraction of the CNTs, the non-dimensional in-plane displacements and transverse displacements are decreasing as the value of the core to face sheet thickness ratio is increasing.

The non-dimensional transverse displacement for different possible distribution combinations of the CNTs in FG-CNTR sandwich plate at the top and bottom face sheet with L2 stacking sequence is obtained and is represented in Table 4.10. The results for non-dimensional transverse deflection of a carbon nanotube reinforced sandwich plate under sinusoidal load are shown here. The results are obtained using analytical and FE method using the non-polynomial shear deformation theories based on the secant function and inverse hyperbolic sine function. For the analysis of non-dimensional transverse deflection of the simply supported carbon nanotube reinforced composite plate different stacking sequence selected from Table 3.6. The material property selected here, is given in Table 3.3 and the non-dimensional parameter selected from sub section 3.11. Uniformly distributed carbon nanotube reinforced composite plate used as top and bottom face sheet along with Titanium alloy (T) as the homogenous core sandwich plate is selected here for the analysis. In CNT reinforced composite plate, M1 is used as the matrix along with the CNTs fibers. The simply supported square CNTR sandwich plate is subjected to sinusoidal load in this analysis. The results are compared with eRTZ results of Sciuva and Sorrenti (2014). The results presented show a good agreement with the existing results available in the literature. In the similar way, non-dimensional transverse displacements for /\-/\, V-V, X-X and O-O sandwich plates are also presented in the table.

In Table 4.11 the non-dimension transverse displacement for the functionally graded carbon nanotube reinforced sandwich plate is presented. L4 and L5 stacking sequence is

selected for the analysis. Here are the findings for the non-dimensional transverse deflection of a sandwich plate reinforced with carbon nanotubes under a sinusoidal load. The non-polynomial shear deformation theories based on the secant function and inverse hyperbolic sine function, are used here to produce non-dimensional transverse deflection analytical and FE method. The non-dimensional transverse deflection of the simply supported carbon nanotube reinforced sandwich plate are obtained for, different stacking sequence selected from Table 3.6. The material property selected here, is given in Table 3.3 and the non-dimensional parameter selected from sub section 3.11. The CNTRC plate is used as the face sheet which consists of CNTs as the fiber and PmPV as matrix and along with this homogenous core layer is made of PmPV polymer. Non-dimensional transverse deflections, for different volume fraction of CNTs and span thickness ratios are evaluated for the simply supported square sandwich plate which is subjected to UDL. FG-T and FG-B distributions are selected for the top and bottom face sheets for CNT distribution. The presented results are compared with the results published by Draoui *et al.* (2019). It is observed from the literature that the selected theories provides a more accurate result as compared to the FSDT with same number of degrees of freedom (5) and also inherently satisfied the traction free boundary condition. It is also observed that the present results show well agreements with the existing results. It is observed from the tables that for a particular core to face sheet thickness ratio, the values of non-dimensional transverse displacements are decreased with the increase in the span thickness ratios for UD and FG distributions of CNTs at the face sheets.

The effect of span thickness ratio on non-dimensional transverse deflections for the different volume fraction of CNTs for simply supported sandwich plate with functionally graded carbon nanotube top and bottom face sheet subjected to sinusoidal

loading condition is shown in Figure 4.12. The investigation is done through the application of analytical modelling of carbon nanotube reinforced composite plate within the context of non-polynomial shear deformation theory based on the inverse hyperbolic sine function. L5 stacking sequence is considered for the analysis in which the CNTRC plate is used as a face sheet which consists of CNTs as the fiber and PmPV as a matrix along with this homogenous core layer is modelled as PmPV polymer. It is observed from the figure that as the volume fraction of the CNTs in sandwich plate is increasing the value of the non-dimensional transverse deflections is decreasing for a particular value of span thickness ratio. With increase in the volume fraction of the CNTs in the sandwich plate, the bending stiffness also increases.

Table 4.9 (a): Non- dimensional in-plane deflection of simply supported square FG-CNTR sandwich plate for L1 stacking sequences

V^*_{cnt}	h_c/h_f	b/h	Present[@]	Present[*]	Present[$]	Present[&]	Natarajan *et al.* (2014) (HSDT)	Natarajan *et al.* (2014)(TOSDT)	Natarajan *et al.* (2014)(FSDT)
0.17	2	5	0.6867	0.9490	0.6921	0.9523	0.6883	0.9108	-
		10	0.8476	0.9450	0.8524	0.9486	0.8721	0.9359	0.9341
	6	5	0.6499	0.7120	0.6532	0.7192	0.6887	0.6840	-
		10	0.6998	0.7060	0.7002	0.7104	0.7010	0.6994	0.6983
0.28	2	5	0.5260	0.6650	0.5326	0.6784	0.4456	0.6314	-
		10	0.5826	0.6600	0.5910	0.6810	0.5979	0.6519	0.6504
	6	5	0.5632	0.5930	0.5672	0.5980	0.5610	0.5671	-
		10	0.5829	0.5930	0.5921	0.6145	0.5835	0.5848	0.5835

Table 4.9 (b): Non- dimensional transverse deflection of simply supported square FG-CNTR sandwich plate for L1 stacking sequences

V^*_{cnt}	h_c/h_f	b/h	Present[@]	Present[*]	Present[$]	Present[&]	Natarajan *et al.* (2014) (HSDT)	Natarajan *et al.* (2014)(TOSDT)	Natarajan *et al.* (2014)(FSDT)
0.17	2	5	0.0842	0.0708	0.0854	0.0721	0.0847	0.0744	-
		10	0.0596	0.0521	0.0621	0.0561	0.0668	0.0637	0.0645
	6	5	0.0522	0.0520	0.0532	0.0532	0.0526	0.0523	-
		10	0.0467	0.0467	0.0484	0.0484	0.0468	0.0467	0.0471
0.28	2	5	0.0701	0.0531	0.0732	0.0565	0.0683	0.0573	-
		10	0.0601	0.0606	0.0621	0.0629	0.0492	0.0458	0.0466
	6	5	0.0448	0.0450	0.0454	0.0462	0.0458	0.0455	-
		10	0.0416	0.0394	0.0451	0.0462	0.0397	0.0396	0.0400

Present[@]- Analytical non-polynomial shear deformation theory based on secant function.
Present[*]- Analytical non-polynomial shear deformation theory based on inverse hyperbolic sine function.
Present[$]- FE modeling using non-polynomial shear deformation theory based on secant function.
Present[&]- FE modeling using non-polynomial shear deformation theory based on inverse hyperbolic sine function.

Table 4.10: Deflection of simply supported square sandwich plate for for L2 stacking sequence

Topography	*b/h*	Present[@]	Present[*]	Present[$]	Present[&]	Sciuva and Sorrenti (2014)
U-U	8	5.6049	5.6509	5.7483	5.7713	5.8943
	10	5.4805	5.534	5.5901	5.6168	5.7016
	20	5.3141	5.3779	5.374	5.4059	5.4347
	50	5.267	5.3342	5.3122	5.3458	5.3577
	100	5.26	5.3279	5.3032	5.3371	5.3466
/\-/\	8	5.6508	5.6049	5.7712	5.7483	5.8917
	10	5.5339	5.4805	5.6168	5.5901	5.6997
	20	5.3777	5.3141	5.4058	5.374	5.434
	50	5.334	5.267	5.3457	5.3122	5.3575
	100	5.3277	5.26	5.337	5.3032	5.3464
V-V	8	5.8917	5.6049	5.8917	5.7483	5.8917
	10	5.6997	5.4805	5.6997	5.5901	5.6997
	20	5.434	5.3141	5.434	5.374	5.434
	50	5.3575	5.267	5.3575	5.3122	5.3575
	100	5.3464	5.26	5.3464	5.3032	5.3464
X-X	8	5.6308	5.592	5.7593	5.7399	5.8878
	10	5.5514	5.467	5.6219	5.5797	5.6924
	20	5.3601	5.3	5.3899	5.3599	5.4198
	50	5.3168	5.254	5.3287	5.2973	5.3407
	100	5.3106	5.247	5.3199	5.2881	5.3293
O-O	8	5.664	5.6212	5.779	5.7576	5.894
	10	5.5462	5.4958	5.6252	5.6	5.7042
	20	5.3889	5.3284	5.4159	5.3857	5.443
	50	5.3448	5.2814	5.3564	5.3247	5.368
	100	5.3385	5.2748	5.3478	5.316	5.3572

Present[@]- Analytical non-polynomial shear deformation theory based on secant function.
Present[*]- Analytical non-polynomial shear deformation theory based on inverse hyperbolic sine function.
Present[$]- FE modeling using non-polynomial shear deformation theory based on secant function.
Present[&]- FE modeling using non-polynomial shear deformation theory based on inverse hyperbolic sine function.

Table 4.11: Non dimensional transverse deflection $\bar{w}_1$ ($a/2$, $b/2$, $h/2$) for simply supported FG-CNTR sandwich plate subjected to the UDL for L4 and L5 stacking sequence

V^*_{cnt}	*b/h*	Type	Draoui et al. (2019)	Present[@]	Present[*]	Present[$]	Present[&]
0.11	10	UD	0.8067	0.7710	0.8470	0.7888	0.8268
		FG	0.7417	0.4208	0.7553	0.5812	0.7485
	20	UD	0.5024	0.4932	0.5435	0.4978	0.5229
		FG	0.4349	0.4208	0.4667	0.4278	0.4508
	50	UD	0.4125	0.4135	0.4556	0.4130	0.4340
		FG	0.3471	0.3445	0.3834	0.3458	0.3652

0.14	10	UD	0.7166	0.6866	0.7596	0.7016	0.7381
		FG	0.6630	0.6158	0.6812	0.6394	0.6721
	20	UD	0.4158	0.4083	0.4551	0.4120	0.4354
		FG	0.3613	0.3491	0.3917	0.3552	0.3765
	50	UD	0.3298	0.3284	0.3666	0.3291	0.3482
		FG	0.2752	0.2731	0.3078	0.2741	0.2915
0.17	10	UD	0.5254	0.5925	0.6454	0.55895	0.5854
		FG	0.4809	0.5292	0.5836	0.5050	0.5322
	20	UD	0.3277	0.3459	0.3797	0.3368	0.3537
		FG	0.2830	0.2956	0.3284	0.2893	0.3057
	50	UD	0.2711	0.2740	0.3019	0.2725	0.2865
		FG	0.2263	0.2281	0.2538	0.2272	0.2400

Present[@]- Analytical non-polynomial shear deformation theory based on secant function.
Present[*]- Analytical non-polynomial shear deformation theory based on inverse hyperbolic sine function.
Present[$]- FE modeling using non-polynomial shear deformation theory based on secant function.
Present[&]- FE modeling using non-polynomial shear deformation theory based on inverse hyperbolic sine function.

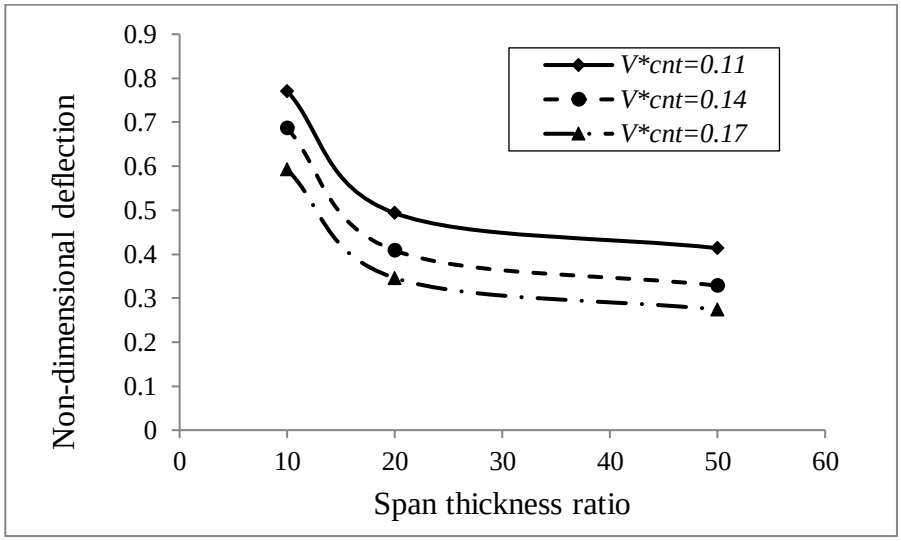

Figure 4.12. Effect of span thickness ratio on non-dimensional transverse deflections for different volume fraction of CNTs

4.3.1.2. Normal stress analysis of the carbon nanotube reinforced sandwich plate

In this section, stress analysis of the carbon nanotube reinforced sandwich plate for different span thickness ratios, core to face sheet ratio and volume fraction for a particular stacking sequence is carried out and the distribution of the normal stress through the thickness of the carbon nanotube reinforced sandwich plate is discussed in detail. The outcome of the analysis is presented in the tabular form in Table 4.12. The

results for non-dimensional normal stresses of a carbon nanotube reinforced sandwich plate under sinusoidal load are shown here. These results are obtained using analytical and FE modelling within the framework of non-polynomial shear deformation theories based on the secant function and inverse hyperbolic sine function. For the analysis of non-dimensional normal stresses of the simply supported carbon nanotube reinforced sandwich plate different stacking sequence selected from Table 3.6. The material properties selected here, is given in Table 3.3 and the non-dimensional parameter selected from sub section 3.11. It is observed from the table that the normal stresses are decreasing for a particular span thickness ratio and volume fraction of the CNTs, for the increasing value of core to face sheet thickness ratios. Similarly, normal stresses are increasing as the span thickness ratio is increasing, for a particular value of the core to face sheet thickness ratio and span thickness ratio. The variation of non-dimensional axial stresses (σ_{xx}) with normalized thickness for the different volume fraction of CNTs is shown in Figure 4.13. The investigation is done through the application of analytical modelling of carbon nanotube reinforced composite plate within the context of non-polynomial shear deformation theory based on the inverse hyperbolic sine function. Here, L5 stacking sequence is considered in which FG-T and FG-B distributions are considered at the top and bottom face sheets of the sandwich plate. CNTs reinforced composite plate is consists of CNTs as fiber and PMMA as a matrix. T is selected for modelling of the homogenous core. The simply supported square sandwich plate is subjected to the sinusoidal loading condition for span thickness ratio of 50 is considered here for the analysis. It is observed from the figure that as the value of the volume fraction of the CNTs is increasing, the bending stiffness of the sandwich plate is increased. The value of the normal stress is maximum at the top and bottom surface of the carbon nanotube reinforced sandwich plate. The stresses are discontinuous at any k^{th}

interface due to dissimilar transformed reduced stiffness coefficients '$\bar{Q}_{ij}$' of the k^{th} and $(k + 1)^{th}$ layer. The variation of non-dimensional axial stresses with normalized thickness for the different core to face sheet thickness ratios are shown in Figure 4.14. The investigation is done through the application of analytical modelling of carbon nanotube reinforced composite plate within the context of non-polynomial shear deformation theory based on the inverse hyperbolic sine function. For the top and bottom face sheets, FG-T and FG-B distributions are considered respectively. The CNTRC plate used as top and bottom face sheet consists of CNTs as fiber and PMMA as a matrix. T is selected as the homogenous core. The span thickness ratio is considered as 50. Simply supported square sandwich plate is subjected to the sinusoidal load is considered here for the analysis. The figure indicates that, as the value of the core to face sheet thickness ratio increases the bending stiffness of the FG-CNTR sandwich plate goes on decrease.

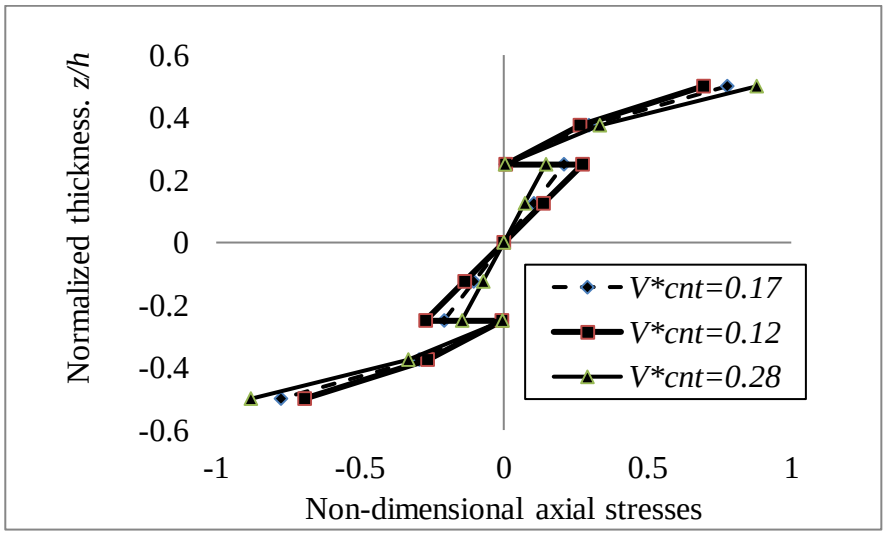

Figure 4.13. Variation of non-dimensional axial stresses (σ_{xx}) with normalized thickness for different volume fraction of CNTs

Table 4.12: Normal stress (σ_{xx}) of simply supported square FG-CNTR sandwich plate for L1 stacking sequences

V^*_{cnt}	h_c/h_f	b/h	Present[@]	Present[*]	Present[$]	Present[&]	Natarajan *et al.* (2014) (HSDT)	Natarajan *et al.* (2014)(TOSDT)	Natarajan *et al.* (2014)(FSDT)
0.17	2	5	0.5627	0.7802	0.5687	0.7688	0.5747	0.7575	-
		10	0.7625	0.7766	0.7440	0.7772	0.7255	0.7779	0.7765
	6	5	0.4982	0.5852	0.5354	0.5769	0.5727	0.5687	-
		10	0.4932	0.5805	0.5379	0.5809	0.5827	0.5813	0.5804
0.28	2	5	0.7254	0.8899	0.66525	0.87205	0.6051	0.8542	-
		10	0.8820	0.8826	0.8453	0.8815	0.8086	0.8810	0.8791
	6	5	0.7932	0.7962	0.77585	0.7799	0.7585	0.7666	-
		10	0.7903	0.7912	0.7894	0.79025	0.7885	0.7902	0.7885

Table 4.13: Transverse shear stress (τ_{xz}) of simply supported square FG-CNTR sandwich plate for L1 and L2 stacking sequences

V^*_{cnt}	h_c/h_f	b/h	Present[@]	Present[*]	Present[$]	Present[&]	Natarajan *et al.* (2014) (HSDT)	Natarajan *et al.* (2014)(TOSDT)	Natarajan *et al.* (2014)(FSDT)
0.17	2	5	0.3807	0.4767	0.3866	0.4282	0.3926	0.3798	-
		10	0.3020	0.4815	0.3445	0.4321	0.3870	0.3828	0.3826
	6	5	0.2997	0.3194	0.3079	0.3174	0.3162	0.3155	-
		10	0.3026	0.3194	0.3105	0.3187	0.3184	0.3181	0.3179
0.28	2	5	0.3910	0.4940	0.3890	0.4332	0.3870	0.3724	-
		10	0.3851	0.5004	0.3829	0.4382	0.3807	0.3760	0.3757
	6	5	0.3160	0.3337	0.3170	0.3252	0.3180	0.3167	-
		10	0.3220	0.3371	0.3214	0.3286	0.3208	0.3202	0.3199

Present[@]- Analytical non-polynomial shear deformation theory based on secant function.
Present[*]- Analytical non-polynomial shear deformation theory based on inverse hyperbolic sine function.
Present[$]- FE modeling using non-polynomial shear deformation theory based on secant function.
Present[&]- FE modeling using non-polynomial shear deformation theory based on inverse hyperbolic sine function.

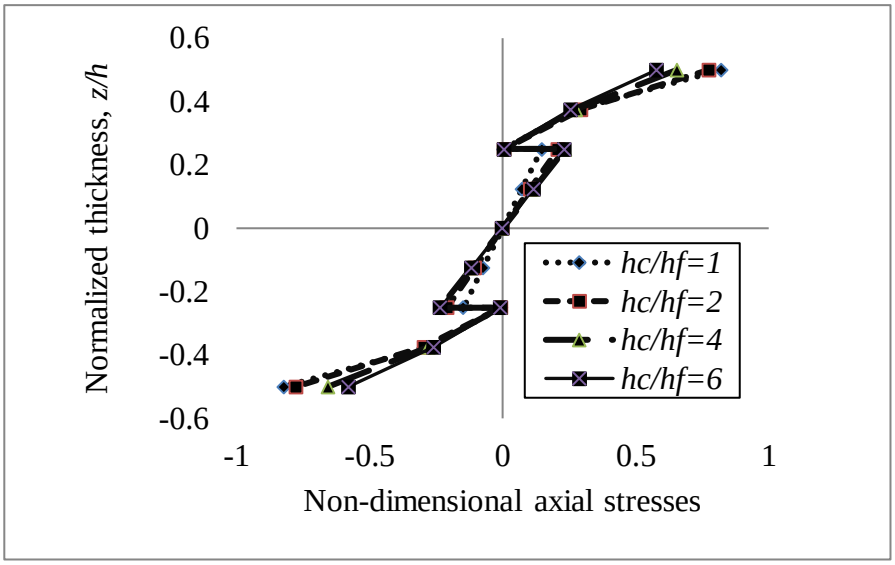

Figure 4.14. Variation of non-dimensional axial stresses (σ_{xx}) with normalized thickness for different core to face sheet thickness

In Figure 4.15, the variation of the non-dimensional axial stresses (σ_{xx}) with normalized thickness for different tropology sequences, in which one has CNTRC plate as core and in another CNTRC plate, is used as top and bottom face sheet is shown. For the top and bottom face sheets of FG-CNTR sandwich plate, FG-T and FG-B distribution are considered respectively. The analytical modelling of carbon nanotube reinforced composite plate using non-polynomial shear deformation theory based on the inverse hyperbolic sine function is used here to obtain the required results. CNTRC plate used as top and bottom face sheet consisting of CNTs as fiber and PMMA as a matrix. T is selected as the homogenous core. In the next case, CNTRC plate as core FG-T distribution is considered for the core in which CNTs are used as fiber and PMMA is used as a matrix. T is modelled as a homogenous top and bottom face sheet. From the figure, it can be observed that for a particular core to face sheet thickness ratio i.e. 2, non-dimensional axial stresses for the core CNTs reinforced plate are higher than that of the face sheet reinforced with CNTs.

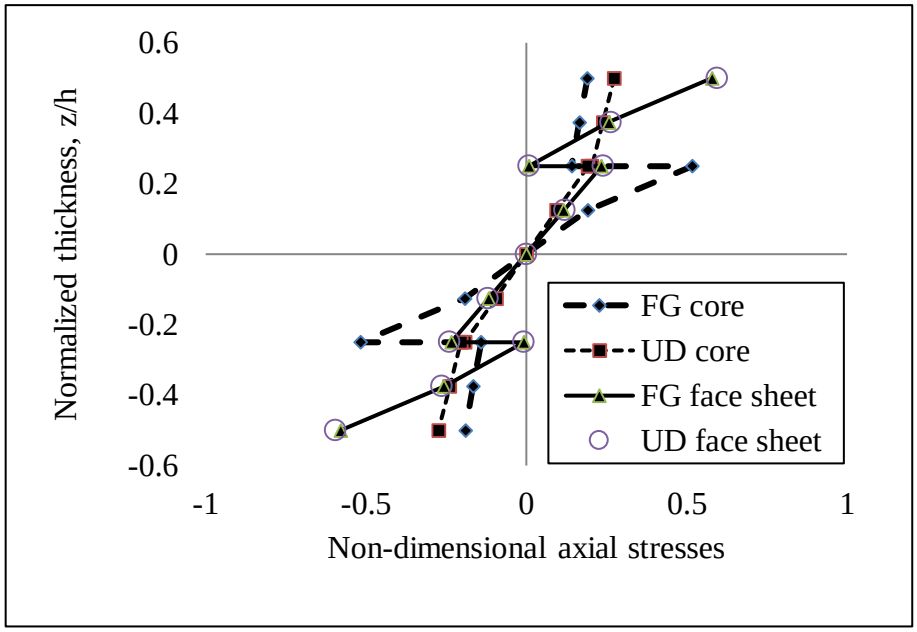

Figure 4.15. Variation of non-dimensional axial stresses with normalized thickness for different tropology sequences

4.3.1.3. Non-dimensional transverse shear stresses of the carbon nanotube reinforced sandwich plate

In this section, non-dimensional transverse shear stresses (τ_{xz}) analysis of the carbon nanotube reinforced sandwich plate for different span thickness ratios, core to face sheet ratio, and volume fraction for a particular stacking sequence is discussed in detail. The results for the analysis are displayed in the Table 4.13**.** Here are the findings for the non-dimensional transverse shear stress of a sandwich plate reinforced with carbon nanotubes under a sinusoidal load. The non-polynomial shear deformation theories based on the secant function and inverse hyperbolic sine function are used to produce the result by utilizing the analytical and FE methods. For the analysis of non-dimensional transverse shear stresses of the simply supported carbon nanotube reinforced sandwich plate, different stacking sequences are selected from Table 3.6. The material property selected here, is given in Table 3.3 and the non-dimensional parameter selected from sub section 3.11. The present results are compared with the Natarajan *et al.* (2014) results which show that the results synchronize well with the

present results. It is very clearly observed from the table that non-dimensional transverse shear stresses are decreasing for a particular span thickness ratio and volume fraction of the CNTs, for the increasing value of core to face sheet thickness ratios.

4.3.2. Free vibration analysis of carbon nanotube reinforced sandwich plate

In this section, free vibration analysis is conducted for the FG-CNTR sandwich plates for different stacking sequences, span thickness ratios, and core to face sheet thickness ratios. The non-dimensional fundamental frequency is investigated for simply supported square FG-CNTR sandwich plate for L3 stacking sequences is presented in Table 4.14. For the analysis of non-dimensional natural frequency of the simply supported carbon nanotube reinforced sandwich plate, different stacking sequence selected from Table 3.6. The material property selected here, is given in Table 3.3 and the non-dimensional parameter selected from sub section 3.11. FG-T and FG-B distributions are considered as the top and bottom face sheet respectively. Titanium alloy (T) is used as the homogenous core in the sandwich plate. The results are derived using analytical and FE method using the non-polynomial shear deformation theories based on the secant function and inverse hyperbolic sine function. The results are compared with the results given by Natarajan *et al.* (2014) and Wang and Shen (2012) which show well agreement with the existing results. It can be observed from the table that as the volume fraction of the CNTs is increasing in the sandwich plate, non-dimensional fundamental frequency is increasing for a fixed span thickness ratio whereas with the increase in span thickness ratio of sandwich plate, the non-dimensional fundamental frequency is increased for a fixed volume fraction of the CNTs. The non-dimensional fundamental frequency depends on the core to face sheet thickness ratios. For smaller core to face sheet thickness ratio, the non-dimensional fundamental frequency is lower as compared to the fundamental frequency obtained for higher core to face sheet thickness ratio. Hence, it

can also be concluded that the non-dimensional fundamental frequency increase as the depth of the homogenous core is increased.

Table 4.14: Non dimensional fundamental frequency for simply supported FG-CNTR sandwich plate subjected to the UDL for L3 stacking sequence

b/h	References	V^*_{cnt} = 0.12	V^*_{cnt} = 0.17	V^*_{cnt} = 0.28
20	Present[@]	4.9106	5.1890	5.6566
	Present[*]	4.9109	5.1896	5.6572
	Present[$]	4.9102	5.1880	5.6538
	Present[&]	4.9110	5.1885	5.6548
	Natarajan *et al.* (2014)[#]	4.9099	5.1871	5.6510
	Natarajan *et al.* (2014)[%]	4.9111	5.1881	5.6524
	Natarajan *et al.* (2014)[!]	4.9066	5.1826	5.6448
	Wang and Shen (2012)	4.9119	5.1905	5.6569
10	Present[@]	4.8278	5.0954	5.5409
	Present[*]	4.8286	5.0963	5.5419
	Present[$]	4.8251	5.0905	5.5295
	Present[&]	4.8278	5.0930	5.5325
	Natarajan *et al.* (2014)[#]	4.8225	5.0857	5.5182
	Natarajan *et al.* (2014)[%]	4.8271	5.0897	5.5232
	Natarajan *et al.* (2014)[!]	4.8100	5.0691	5.4952
5	Present[@]	4.5613	4.7963	5.1747
	Present[*]	4.5626	4.7973	5.1756
	Present[$]	4.5412	4.7682	5.1260
	Present[&]	4.5495	4.7753	5.1345
	Natarajan *et al.* (2014)[#]	4.5212	4.7402	5.0774
	Natarajan *et al.* (2014)[%]	4.5365	4.7534	5.0935
	Natarajan *et al.* (2014)[!]	4.4820	4.6891	5.0097

Present[@]- Analytical non-polynomial shear deformation theory based on secant function.
Present[*]- Analytical non-polynomial shear deformation theory based on inverse hyperbolic sine function.
Present[$]- FE modeling using non-polynomial shear deformation theory based on secant function.
Present[&]- FE modeling using non-polynomial shear deformation theory based on inverse hyperbolic sine function. [#]HSDT, [%]TOSDT, and [!]FSDT

The Figure 4.16 shows the first six free vibration mode shapes of the simply supported square sandwich plate. FG-T and FG-B distributions are considered as the top and bottom face sheet respectively. Titanium alloy (T) is used as the homogenous core in the FG-CNTR sandwich plate. The corresponding mode shapes are obtained for the carbon nanotube reinforced sandwich plate with span thickness ratio of 20 and core to face sheet thickness ratio of 6. The investigation is done through the application of

analytical modelling of carbon nanotube reinforced composite plate using the non-polynomial shear deformation theory based on the inverse hyperbolic sine function.

eig = 5.189

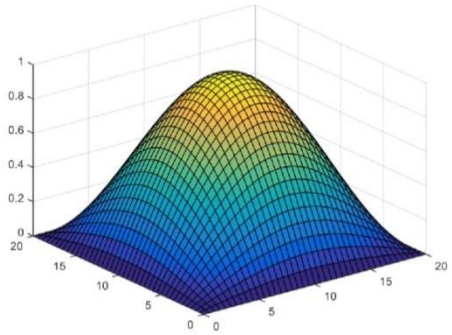

(a)

eig = 11.189

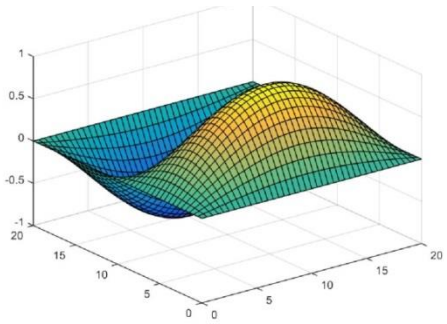

(b)

eig = 15.461

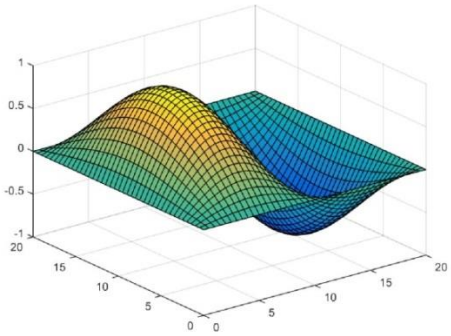

(c)

eig = 20.381

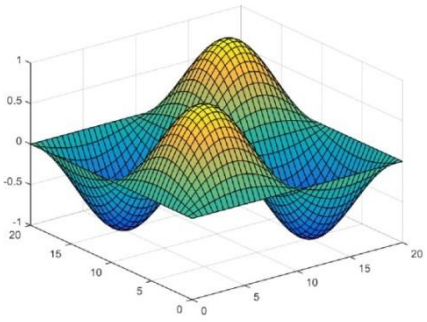

(d)

eig = 21.625

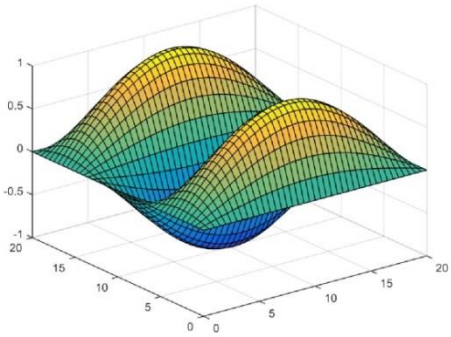

(e)

eig = 29.67

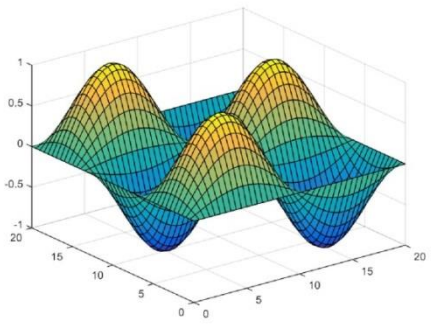

(f)

Figure 4.16. The free vibration mode shape of FG-CNTR sandwich plate. (a) 1st Mode (m = 1, n = 1); (b) 2nd Mode (m = 1, n = 2); (c) 3rd Mode (m = 2, n = 1); (d) 4th Mode (m = 2, n = 2); (e) 5th Mode (m = 1, n = 3); (f) 6th Mode (m = 2, n = 3)

4.4. Structural analysis of functionally graded carbon nanotube reinforced composite plates resting on Pasternak's elastic foundation

In this section, the bending, buckling, and free vibration responses of the functionally graded carbon nano tube reinforced composite plate resting on the Pasternak elastic foundation with shear layer and Winkler springs are presented. The plate is modelled in the framework of non-polynomial shear deformation theory based upon secant function and inverse hyperbolic sine function. These shear deformation theories fulfil the traction free boundary conditions at the top and bottom of the plate. Hamilton's principle is applied to obtain the governing differential equations of the functionally graded carbon nano tube reinforced composite plate resting on the Pasternak's elastic foundation. Navier's technique and FE modelling is applied to obtain the solution for the simply supported boundary condition. The bending, buckling, and free vibration responses of the functionally graded carbon nano tube reinforced composite plate resting on the Pasternak elastic foundation is carried out for different parametric conditions such as volume fraction of CNTs, distribution pattern of CNTs, side thickness ratio and spring constant factors. The analytical and FE results are obtained by implementing both the theories. The bending, buckling, and free vibration responses of plate are investigated in detail and the accuracy of the obtained results are verified numerically by comparing with published results of literature.

4.4.1. Bending analysis of functionally graded carbon nanotube reinforced composite plates resting on Pasternak's elastic foundation

The bending responses of the functionally graded carbon nano tube reinforced composite plate resting on the Pasternak's elastic foundation includes the detail analysis of the transverse deflection, normal stresses and shear stresses is carried out in the

subsections. The parametric effect for different volume fraction of CNTs, distribution pattern of CNTs, side thickness ratio and spring constant factors is analyzed and discussed in detail.

4.4.1.1. Transverse deflection of functionally graded carbon nanotube reinforced composite plates resting on Pasternak's elastic foundation

The dimensionless transverse deflections of CNTRC plate with and without Pasternak's elastic foundation are presented in Table 4.15. The dimensionless transverse deflection of CNTRC plate is investigated for different volume fraction of CNTs, different distribution pattern of CNTs, and different spring constant factors under sinusoidal loading condition are obtained based on the analytical and FE modeling in the framework of non-polynomial shear deformation theories based on the secant function and inverse hyperbolic sine function. For the analysis of non-dimensional transverse deflection of the simply supported carbon nanotube reinforced composite plate resting on Pasternak's elastic foundation, different distribution of carbon nanotube reinforcement pattern is selected from Table 3.1. The material property selected here, is given in Table 3.3 and the non-dimensional parameter selected from sub section 3.11. The obtained analytical and FE deflection results are compared with the available deflection results which were given by Wattanasakulpong and Chaikittiratana (2015). Wattanasakulpong and Chaikittiratana (2015) used TSDT and SSDT to estimate the transverse deflection of CNTRC plate with and without Pasternak's elastic foundation. The obtained results are very closely agreed with the given results of Wattanasakulpong and Chaikittiratana (2015) for side to thickness ratio of 10. From the table it is observed that the FG-X reinforcement distribution of CNTs in the composite plate with and without Pasternak elastic foundation counters the bending reactions very well by producing the minimum transverse deflection in comparison to the other reinforcement

distribution i.e. UD, FG-O, and FG-V selected for the analysis. It is found from the table that by increasing the Winkler spring constant factors and shear layer spring constant factors the stiffness of the system increases due to which the transverse deflection of CNTRC plate with Pasternak elastic foundation decreases. The stiffness of the CNTRC plate for different distribution pattern of CNTs can also be increased by increasing the volume fraction of CNTs.

The effect of variation of the side to thickness ratio on the non-dimensional transverse deflection for the CNTRC plate resting on the Pasternak's elastic foundation is shown in Figure 4.17. The variation is considered here for different distribution pattern of CNTs with the volume fraction of CNTs as 0.14, and Winkler spring constant factors and shear layer spring constant factors of 100 and 50, respectively. The analysis is performed with the application of FE modelling of carbon nanotube reinforced composite plate using non-polynomial shear deformation theory based on secant function. From the figure, it is observed that the FG-X reinforcement distribution of CNTs in the composite plate with Pasternak elastic foundation produces the minimum transverse deflection followed by UD, FG-V, and FG-O reinforcement distribution.

The effect of variation of Winkler spring constant factors and shear layer spring constant factors on the non-dimensional transverse deflection for the CNTRC plate resting on the Pasternak elastic foundation is shown in Figure 4.18. The analysis is carried out with the application of FE modelling of carbon nanotube reinforced composite plate using non-polynomial shear deformation theory based on secant function. The variation is considered here for the side to thickness ratio of 10 with the FG-X distribution pattern of CNTs, and of volume fraction of CNTs of 0.17. It is observed from the figure that by increasing the Winkler spring constant factors and

shear layer spring constant factors the stiffness of the system increases due to which the transverse deflection of CNTRC plate with Pasternak's elastic foundation decreases.

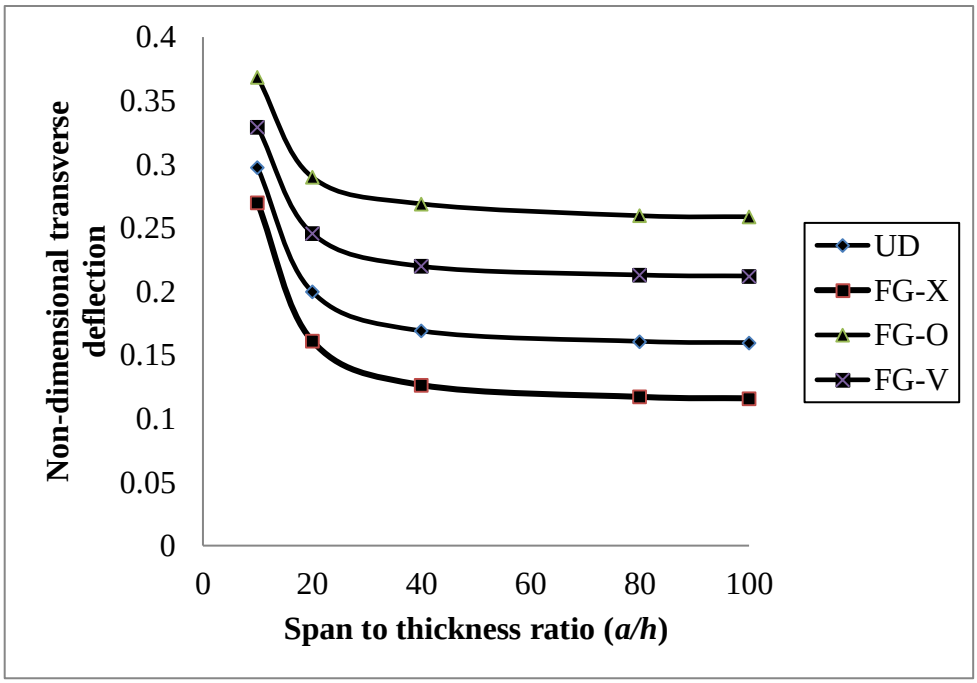

Figure 4.17. Effect of side to thickness ratio on non-dimensional transverse deflection

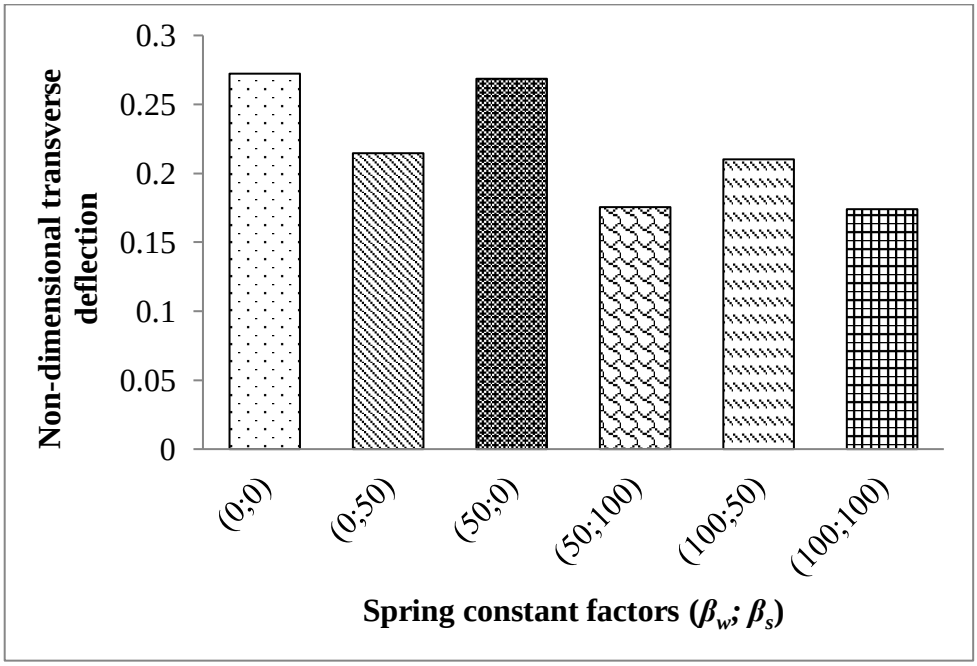

Figure 4.18. The effect of different spring constant factors on non-dimensional transverse deflection

Table 4.15: Dimensionless deflection of CNTRC plate with and without elastic foundation

β_w	β_s		V^*_{CNT} = 0.11				V^*_{CNT} = 0.14				V^*_{CNT} = 0.17			
			UD	**X**	**O**	**V**	**UD**	**X**	**O**	**V**	**UD**	**X**	**O**	**V**
0	0	Present[@]	0.4963	0.4227	0.7080	0.5869	0.4395	0.3817	0.6147	0.5132	0.3176	0.2722	0.4525	0.3768
		Present[*]	0.4869	0.4103	0.7122	0.5779	0.4296	0.3699	0.6176	0.5040	0.3117	0.2658	0.4538	0.3715
		Present[$]	0.4964	0.4235	0.7104	0.5866	0.4396	0.3824	0.6167	0.5130	0.3176	0.2726	0.4532	0.3765
		Present[&]	0.4936	0.4202	0.7113	0.5839	0.4368	0.3793	0.6168	0.5103	0.3159	0.2707	0.4530	0.3749
		Ref (2015)[^]	0.4964	0.4227	0.7081	0.5869	0.4396	0.3817	0.6148	0.5133	0.3177	0.2723	0.4526	0.3769
		Ref (2015)[#]	0.4953	0.4208	0.7104	0.5859	0.4383	0.3800	0.6168	0.5121	0.3170	0.2715	0.4537	0.3763
100	0	Present[@]	0.4729	0.4055	0.6612	0.5543	0.4210	0.3676	0.5791	0.4882	0.3078	0.2651	0.4329	0.3631
		Present[*]	0.4643	0.3941	0.6649	0.5464	0.4119	0.3567	0.5816	0.4798	0.3028	0.2590	0.4341	0.3582
		Present[$]	0.4729	0.4063	0.6633	0.5541	0.4211	0.3683	0.5809	0.4880	0.3078	0.2653	0.4336	0.3628
		Present[&]	0.4704	0.4032	0.6641	0.5839	0.4185	0.3654	0.5810	0.4859	0.3062	0.2636	0.4334	0.3613
		Ref (2015)[^]	0.4729	0.4056	0.6612	0.5544	0.4210	0.3677	0.5792	0.4882	0.3079	0.2651	0.4330	0.3632
		Ref (2015)[#]	0.4719	0.4038	0.6633	0.5534	0.4199	0.3661	0.5809	0.4872	0.3072	0.2644	0.4340	0.3626
100	50	Present[@]	0.3224	0.2896	0.4001	0.3583	0.2974	0.2697	0.3685	0.3294	0.2361	0.2101	0.3033	0.2673
		Present[*]	0.3184	0.2837	0.4014	0.3549	0.2928	0.2638	0.3695	0.3256	0.2328	0.2062	0.3039	0.2646
		Present[$]	0.3223	0.2899	0.4008	0.3581	0.2974	0.2701	0.3691	0.3293	0.2361	0.2102	0.3036	0.2671
		Present[&]	0.3212	0.2884	0.4011	0.3571	0.2961	0.2685	0.3692	0.3282	0.2351	0.2091	0.3035	0.2663
		Ref (2015)[^]	0.3224	0.2896	0.4001	0.3583	0.2974	0.2698	0.3685	0.3295	0.2361	0.2101	0.3034	0.2674
		Ref (2015)[#]	0.3219	0.2888	0.4009	0.3579	0.2969	0.2689	0.3692	0.3290	0.2357	0.2097	0.3039	0.2671

Present[@]- Analytical non-polynomial shear deformation theory based on secant function. Present[*]- Analytical non-polynomial shear deformation theory based on inverse hyperbolic sine function. Present[$]- FE modeling using non-polynomial shear deformation theory based on secant function.Present[&]- FE modeling using non-polynomial shear deformation theory based on inverse hyperbolic sine function. [Ref (2015)]-Wattanasakulpong and Chaikittiratana (2015) ^tsdt #ssdt

4.4.1.2. Non-dimensional stress analysis of functionally graded carbon nanotube reinforced composite plates resting on Pasternak's elastic foundation

In, this section non-dimensional stress analysis i.e., normal stresses, in plane shear stress, and transverse shear stresses for carbon nanotube reinforced composite plate resting on Pasternak's elastic foundation is carried out in detail. The selected analysis is focus on the variation of distribution of carbon nanotubes, volume fraction of carbon nanotubes, and different Winkler layer and shear layer constant factor. Non-dimensional stresses for carbon nanotube reinforced composite plate resting on Pasternak's elastic foundation are shown in Table 4.16 (a) and Table 4.16 (b). To obtain the non-dimensional stresses of the simply supported carbon nanotube reinforced composite plate resting on Pasternak's elastic foundation, different distribution of carbon nanotube reinforcement pattern is selected from Table 3.1. The material property selected here, is given in Table 3.3 and the non-dimensional parameter selected from sub section 3.11. The analytical analysis of the system is carried out in the framework of non-polynomial shear deformation theories based on the inverse hyperbolic sine function and secant function when subjected to a sinusoidal load. From the table 4.16 (a) and 4.16 (b) it is observed that for a particular volume fraction of CNTs, the normal stress (σ_{xx}) due to transverse sinusoidal load is minimum for FG-O distribution and maximum for FG-V distribution. Next, as the value of the volume fraction of CNTs in carbon nanotube reinforced composite plate increases, the non-dimensional in plane shear stresses decreases. Furthermore, it is observed from the tables that for a particular volume fraction of carbon nanotube and span thickness ratio, FG-O distribution show maximum in plane shear stresses as compared to the FG-X which show minimum in plane shear stresses. The FG-O distribution show maximum non-dimensional transverse shear stress as compared with the FG-X which show minimum non-dimensional

transverse shear stresses. For the analysis of the elastic foundation different Winkler spring and shear layer constant factors are chosen and it can be seen from the tables that as the value of the Winkler spring and shear layer constant factor increases, non-dimensional axial stress (σ_{xx}) decreases.

Table 4.16 (a): Non-dimensional stress for carbon nanotube reinforced composite plate resting on elastic foundation using non-polynomial shear deformation theory based on the inverse hyperbolic sine function

Volume fraction	Distribution	β_w	β_s	σ_{xx}	τ_{xy}	τ_{xz}	τ_{yz}
0.11	UD	0	0	0.6571	0.0156	0.4709	0.0384
		100	0	0.6262	0.0149	0.4487	0.0366
		100	50	0.4276	0.0102	0.3065	0.025
	FG-O	0	0	0.0448	0.0223	0.5823	0.0601
		100	0	0.0418	0.0208	0.5436	0.0561
		100	50	0.0253	0.0126	0.3284	0.0339
	FG-X	0	0	0.9015	0.0142	0.4233	0.0314
		100	0	0.8651	0.0136	0.4063	0.0301
		100	50	0.6188	0.0097	0.2906	0.0216
	FG-V	0	0	1.2435	0.0203	0.4615	0.0477
		100	0	1.1749	0.0192	0.4360	0.0451
		100	50	0.7606	0.0124	0.2823	0.0292
0.14	UD	0	0	0.6824	0.0140	0.4709	0.0347
		100	0	0.6539	0.0134	0.4512	0.0333
		100	50	0.4627	0.0095	0.3193	0.0236
	FG-O	0	0	0.0382	0.0191	0.6018	0.0537
		100	0	0.0360	0.0180	0.5668	0.0506
		100	50	0.0229	0.0114	0.3603	0.0322
	FG-X	0	0	0.9444	0.0135	0.4158	0.0290
		100	0	0.9098	0.0130	0.4006	0.0279
		100	50	0.6686	0.0096	0.2944	0.0206
	FG-V	0	0	1.3050	0.0187	0.4626	0.0427
		100	0	1.2416	0.0178	0.4402	0.0406
		100	50	0.8393	0.0120	0.2976	0.0275
0.17	UD	0	0	0.6532	0.0159	0.4708	0.0390
		100	0	0.6332	0.0154	0.4564	0.0378
		100	50	0.4862	0.0118	0.3505	0.0291
	FG-O	0	0	0.0364	0.0211	0.6103	0.0619
		100	0	0.0348	0.0202	0.5838	0.0592
		100	50	0.0244	0.0142	0.4089	0.0415
	FG-X	0	0	0.9077	0.0160	0.4108	0.0323
		100	0	0.8838	0.0156	0.4000	0.0315
		100	50	0.7013	0.0124	0.3174	0.0250
	FG-V	0	0	1.2429	0.0224	0.4602	0.0489
		100	0	1.1980	0.0216	0.4436	0.0472
		100	50	0.8830	0.0159	0.3270	0.0348

Table 4.16 (b): Non-dimensional stress for carbon nanotube reinforced composite plate resting on Pasternak's elastic foundation using non-polynomial shear deformation theory based on the secant function

Volume fraction	Distribution	β_w	β_s	σ_{xx}	τ_{xy}	τ_{xz}	τ_{yz}
0.11	UD	0	0	0.6641	0.0157	0.4423	0.0359
		100	0	0.6327	0.0150	0.4214	0.0342
		100	50	0.4313	0.0102	0.2873	0.0234
	FG-V	0	0	1.2567	0.0204	0.4332	0.0445
		100	0	1.1871	0.0193	0.4092	0.0420
		100	50	0.7674	0.0125	0.2646	0.0272
	FG-X	0	0	0.9171	0.0143	0.3981	0.0290
		100	0	0.8799	0.0137	0.3819	0.0278
		100	50	0.6280	0.0098	0.2726	0.0199
	FG-O	0	0	0.0447	0.0222	0.5310	0.0566
		100	0	0.0418	0.0207	0.4958	0.0529
		100	50	0.0252	0.0125	0.2997	0.0320
0.14	UD	0	0	0.6915	0.0141	0.4434	0.0325
		100	0	0.6623	0.0135	0.4247	0.0311
		100	50	0.4678	0.0096	0.3000	0.0220
	FG-V	0	0	1.3220	0.0189	0.4350	0.0398
		100	0	1.2575	0.0179	0.4138	0.0379
		100	50	0.8486	0.0121	0.2793	0.0256
	FG-X	0	0	0.9629	0.0137	0.3900	0.0267
		100	0	0.9275	0.0132	0.3756	0.0258
		100	50	0.6801	0.0097	0.2755	0.0189
	FG-O	0	0	0.0382	0.0191	0.5521	0.0509
		100	0	0.0359	0.0180	0.5201	0.0480
		100	50	0.0228	0.0114	0.3306	0.0305
0.17	UD	0	0	0.6599	0.0160	0.4422	0.0365
		100	0	0.6396	0.0155	0.4285	0.0354
		100	50	0.4905	0.0119	0.3287	0.0271
	FG-V	0	0	1.2552	0.0225	0.4313	0.0456
		100	0	1.2096	0.0217	0.4156	0.0440
		100	50	0.8906	0.0160	0.3060	0.0324
	FG-X	0	0	0.9208	0.0161	0.3823	0.0296
		100	0	0.8964	0.0157	0.3722	0.0288
		100	50	0.7103	0.0124	0.2949	0.0228
	FG-O	0	0	0.0364	0.0211	0.5616	0.0590
		100	0	0.0348	0.0202	0.5372	0.0564
		100	50	0.0244	0.0142	0.3763	0.0396

Next, the variation of the normal stresses through the thickness of the functionally graded carbon nanotube reinforced composite plates resting on Pasternak's elastic foundation is discussed in detail. For the analysis of simply supported carbon nanotube

reinforced composite plate resting on Pasternak's elastic foundation, different distribution of carbon nanotube reinforcement pattern is selected from Table 3.1. The material property selected here, is given in Table 3.3 and the non-dimensional parameter selected from sub section 3.11. The effect of variation of non-dimensional axial stress (σ_{xx}) across the thickness of CNTRC plate resting on the Pasternak's elastic foundation is shown in Figure 4.19. The analysis is performed using FE method within the framework of non-polynomial shear deformation theory based on secant function. The variation is considered here for the side to thickness ratio of 10 along with the different distribution pattern of CNTs. The volume fraction of CNTs is taken as 0.11 along with the Winkler spring constant factors and shear layer spring constant factors as 100 and 50, respectively. It is observed from the figure that for the symmetrical distribution patterns of CNTs i.e. UD, FG-X, and FG-O across the mid plane of the plate, the axial stress profile is also symmetrical whereas, for the un-symmetrical distribution patterns of CNTs i.e. FG-V reinforced CNTRC plate, axial stress profile is also un-symmetrical. It is observed from the figure that the CNTs distribution patterns across the thickness of the plate effects the variation of the axial stress across the thickness of the plate. The distribution of CNTs for FG-V, the CNTs concentration is maximum at the top of the plate and approaches to zero at the bottom of the plate due to which the axial stress profile shows maximum axial stress at the top of the plate whereas, it approaches to zero at the bottom of the plate. Similarly, for FG-O distribution, the CNTs concentration approaches to zero at the top and bottom of the plate due to which the axial stress profile approaches to zero at the top and bottom of the plate, respectively. It can be observed from the figure that the axial stress profile is zero at the mid plane of the CNTRC plate for UD, FG-X, and FG-O distribution of CNTs whereas, it is non-zero for FG-V distribution. This happened because of the

symmetrical distribution patterns of CNTs in the case of UD, FG-X, and FG-O across the mid plane of the plate and un-symmetrical distribution patterns of CNTs for FG-V across the mid plane of the plate, respectively.

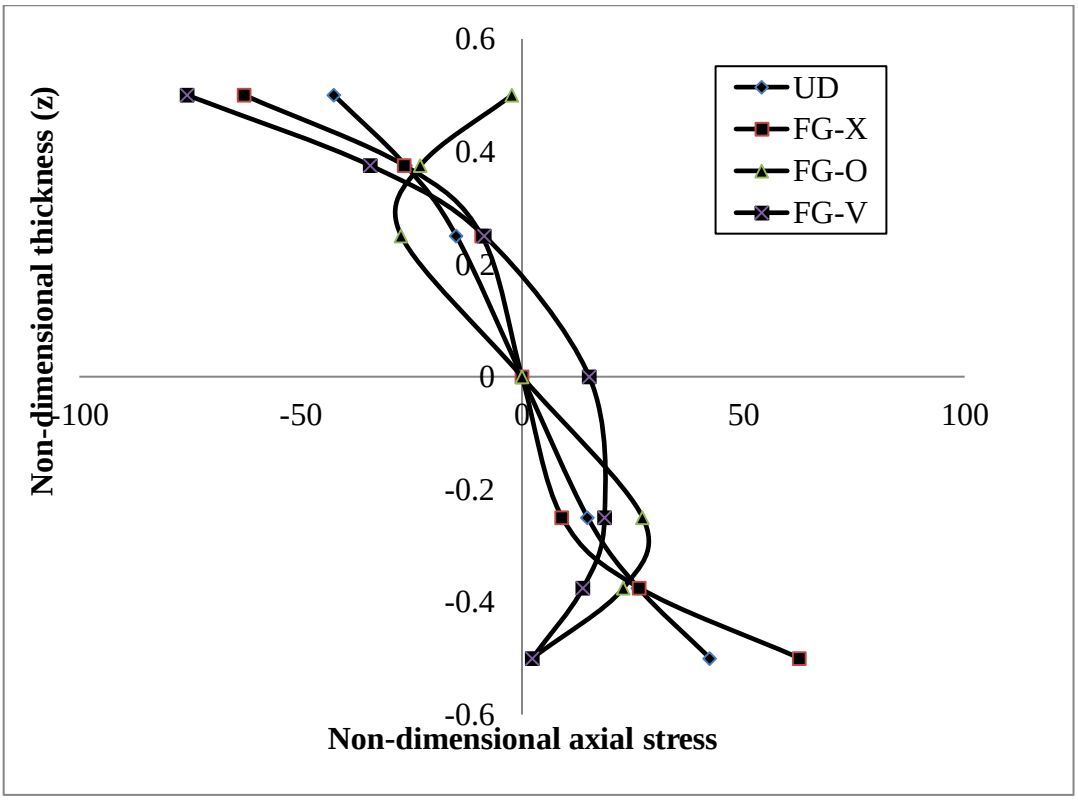

Figure 4.19. The variation of non-dimensional axial stress (σ_{xx}) across the thickness of CNTRC plate resting on the Pasternak elastic foundation for different distribution of CNTs

In Figure 4.20**,** the investigation is done through the application of analytical modelling of carbon nanotube reinforced composite plate within the context of non-polynomial shear deformation theory based on secant function. The variation of non-dimensional axial stress (σ_{xx}) across the thickness of CNTRC plate resting on the Pasternak's elastic foundation for FG-X CNTs distribution with different Winkler spring constant factors and shear layer spring constant factors are shown. It can be observed from the figure that Winkler spring constant factors and shear layer spring constant factors effects the

variation of the axial stress across the thickness of plate, as the value of spring constant factors increases the value of the non-dimensional axial stress decreases.

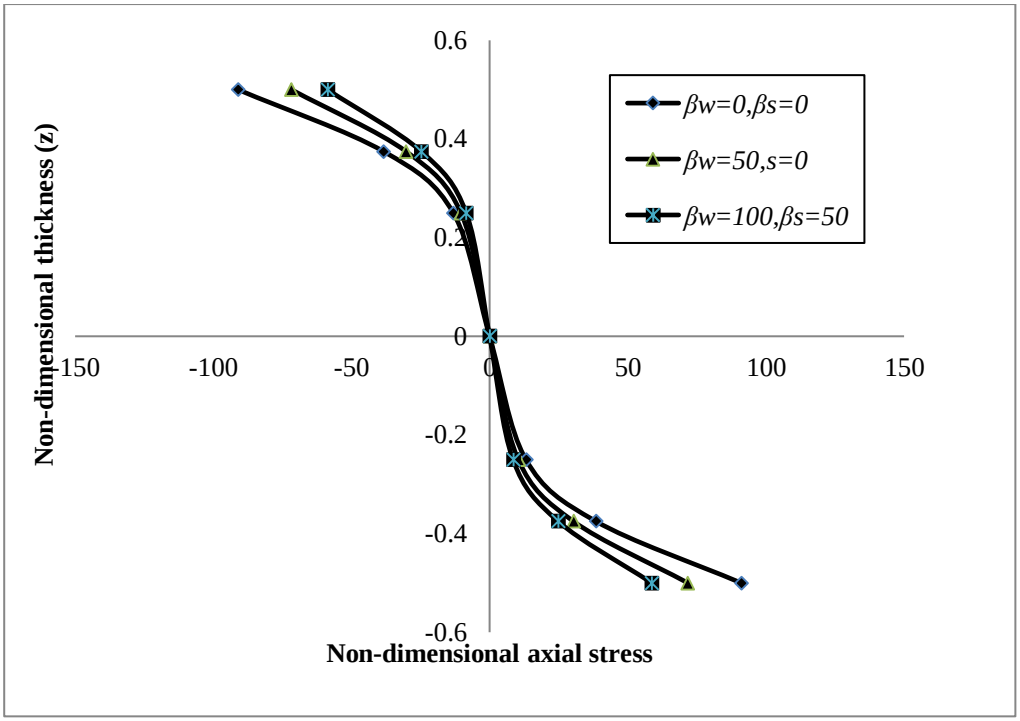

Figure 4.20. The variation of non-dimensional axial stress (σ_{xx}) across the thickness of CNTRC plate resting on the Pasternak elastic foundation for FG-X CNTs distribution with different spring constant factors

The effect of variation of non-dimensional transverse shear stress (τ_{yz}) across the thickness of CNTRC plate resting on the Pasternak elastic foundation is shown in Figure 4.21. The stress analysis is carried out with the application of FE modelling of carbon nanotube reinforced composite plate using the non-polynomial shear deformation theory based on secant function. The variation is considered here for the side to thickness ratio of 10 with the different distribution pattern of CNTs. The volume fraction of CNTs is considered here as 0.14 along with the Winkler spring constant factors and shear layer spring constant factors as 100 and 50, respectively. It is observed from the figure that for the symmetrical distribution patterns of CNTs i.e. UD, FG-X, and FG-O across the mid plane of the plate, the non-dimensional transverse shear stress profile is also symmetrical whereas, for un-symmetrical distribution patterns of CNTs

i.e. FG-V reinforced CNTRC plate, non-dimensional transverse shear stress profile is also un-symmetrical. It is observed from the figure that the CNTs distribution patterns across the thickness of the plate affect the variation of the non-dimensional transverse shear stress across the thickness of the plate. The non-dimensional transverse shear stress is maximum for the FG-O distribution and minimum for FG-X distribution of CNTs.

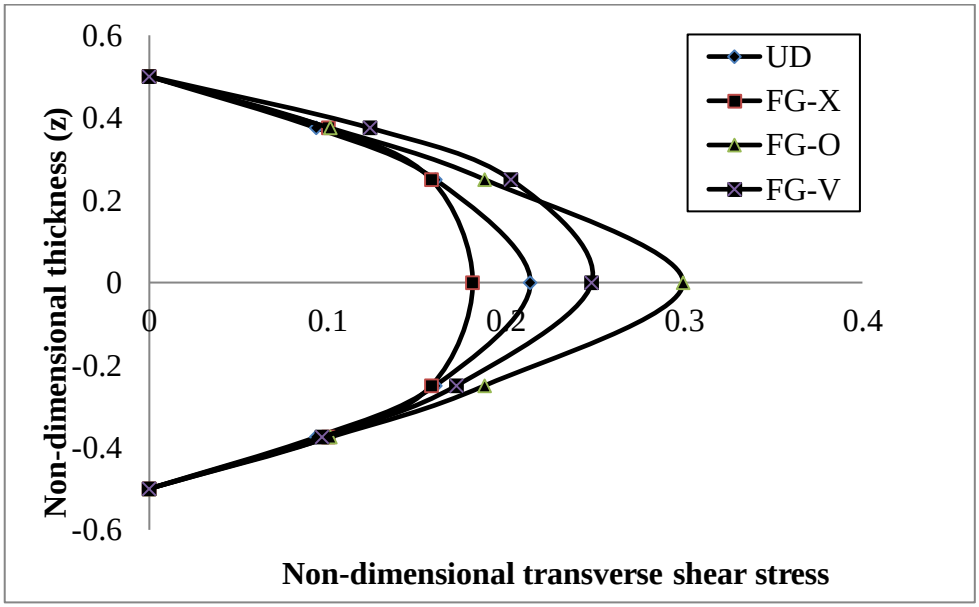

Figure 4.21. The effect of variation of non-dimensional transverse shear stress (τ_{yz}) across the thickness of CNTRC plate resting on the Pasternak elastic foundation for different distribution of CNTs

4.4.2. Free vibration analysis of functionally graded Carbon nanotube reinforced composite plates resting on Pasternak elastic foundation

In this section, the free vibration analysis of the CNTRC plate resting on Pasternak's elastic foundation is discussed in detail. The free vibration analysis of the carbon nanotube reinforced composite plates resting on the Pasternak's elastic foundation includes the natural frequencies and the higher modes of vibration of the plates due to variation of the different parametric conditions which mainly incorporates the variation of the reinforcement distribution pattern of carbon nanotubes across the thickness of the carbon nanotube reinforced composite plate, volume fraction of carbon

nanotubes in carbon nanotube reinforced composite plate, Winkler spring constant factor, shear layer constant factor, and side to thickness ratios.

The dimensionless natural frequency of CNTRC plate with and without Pasternak elastic foundation are obtained based on the analytical and FE modeling in the framework of non-polynomial shear deformation theories based on the secant function and inverse hyperbolic sine function which are shown in Table 4.16. For the analysis of non-dimensional natural frequency of the simply supported carbon nanotube reinforced composite plate resting on Pasternak's elastic foundation, different distribution of carbon nanotube reinforcement pattern is selected from Table 3.1. The material property selected here, is given in Table 3.3 and the non-dimensional parameter selected from sub section 3.11. The dimensionless natural frequency of CNTRC plate with and without Pasternak elastic foundation is presented here for different volume fraction of CNTs, different distribution pattern of CNTs, and different spring constant factors. It is observed that the present results for dimensionless natural frequency agreed very well with the published solution of Wattanasakulpong and Chaikittiratana (2015). The dimensionless natural frequency of CNTRC plate with and without Pasternak elastic foundation is estimated for the side to thickness ratio of 10. From the table, it is observed that the FG-X reinforcement distribution of CNTs in the composite plate with and without Pasternak elastic foundation produces higher natural frequency which is followed by UD, FG-V, and FG-O reinforcement distribution. It is found from the table that by increasing the Winkler spring constant factors and shear layer spring constant factors, the dimensionless natural frequency of the CNTRC plate increases. The dimensionless natural frequencies of the CNTRC plate for different distribution pattern of CNTs are also increased by increasing the volume fraction of CNTs.

First six mode shapes for the frequency are shown in Figure 4.22 for of simply supported CNTRC plate resting on the Pasternak elastic foundation considered here as the erlier problem. The mode shapes are drawn for the FG-O distribution of CNTs with volume fraction of CNTs as 0.14 and side to thickness ratio of 10. The Winkler springs constant factors and shear layer spring constant factors is selected as 100 and 50, respectively. The investigation is done through the application of analytical modelling of carbon nanotube reinforced composite plate using the non-polynomial shear deformation theory based on secant function.

4.4.3. Buckling analysis of functionally graded carbon nanotube reinforced composite plates resting on Pasternak's elastic foundation

In this section, the buckling analyses of the CNTRC plate with Pasternak's elastic foundation under uniaxial and biaxial compressive loads are discussed in detail. The detailed buckling response of the carbon nanotube reinforced composite plates resting on the Pasternak's elastic foundation is explored due to the variation of the different parametric conditions which mainly incorporates the variation of the reinforcement distribution pattern of carbon nanotubes across the thickness of the carbon nanotube reinforced composite plate, volume fraction of carbon nanotubes in carbon nanotube reinforced composite plate, Winkler spring constant factor, shear layer constant factor, and side to thickness ratios.

4.4.3.1. Buckling analysis of uni-axially loaded functionally graded carbon nanotube reinforced composite plates resting on Pasternak's elastic foundation

The dimensionless critical buckling load under uniaxial compressive load (Ψ_x= -1, Ψ_y= 0) of CNTRC plate with and without Pasternak's elastic foundation are obtained using analytical and FE methods in the framework of non-polynomial shear deformation theories based on the secant function and inverse hyperbolic sine function is shown in

Table 4.17. To obtain the non-dimensional buckling load of the simply supported uni-axially loaded carbon nanotube reinforced composite plate resting on Pasternak's elastic foundation, different distribution of carbon nanotube reinforcement pattern is selected from Table 3.1. The material property selected here, is given in Table 3.3 and the non-dimensional parameter selected from sub section 3.11. The dimensionless critical buckling load under uniaxial compressive load is evaluated for different volume fraction of CNTs, different distribution pattern of CNTs, and different spring constant factors. The presented dimensionless critical buckling loads are compared with the available results which were given by Wattanasakulpong and Chaikittiratana (2015). The results are agreed well with the present result for side to thickness ratio of 10. From the table, it is observed that the FG-X reinforcement distribution of CNTs in the composite plate with and without Pasternak's elastic foundation resist the uniaxial compressive load very well by giving the maximum value of dimensionless critical buckling load which is followed by UD and FG-O reinforcement distribution. It can be observed from the table that, as the Winkler spring constant factors and shear layer spring constant factors increases, the stiffness of the system in the lateral direction increases due to which the dimensionless critical buckling load increases for the CNTRC plate with Pasternak elastic foundation. The stiffness of the system in the lateral direction can also be increased by increasing the volume fraction of CNTs in the composite plate due to which the dimensionless critical buckling load increases for the CNTRC plate with Pasternak's elastic foundation.

The effect of variation of Winkler spring constant factors and shear layer spring constant factors on non-dimensional critical buckling load of CNTRC plate with Pasternak's elastic foundation for UD reinforcement distribution pattern is shown in the Figure 4.23. The investigation is done through the application of analytical modelling of

carbon nanotube reinforced composite plate within the context of non-polynomial shear deformation theory based on secant function. The analysis is conducted for the different volume fraction of CNTs, Winkler spring constant factors and shear layer spring constant factors. It is observed from the figure that for a specific volume fraction of CNTs, the value of the non-dimensional critical buckling load increases as the value of the Winkler spring constant factors and shear layer spring constant factors increases. Similarly, for a specific Winkler spring constant factors and shear layer spring constant factors, the value of the non-dimensional critical buckling increases with the increase in the volume fraction of CNTs.

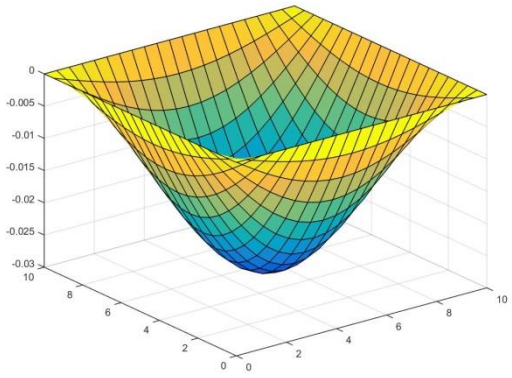

(a)

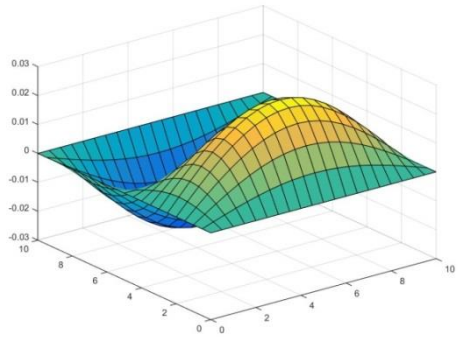

(b)

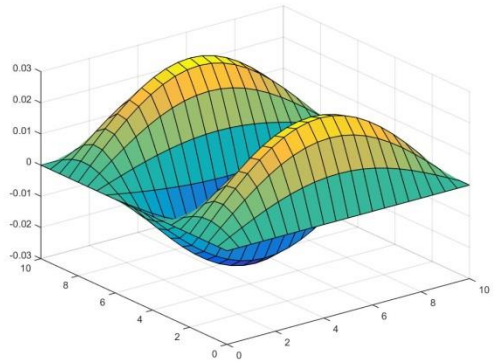

(c)

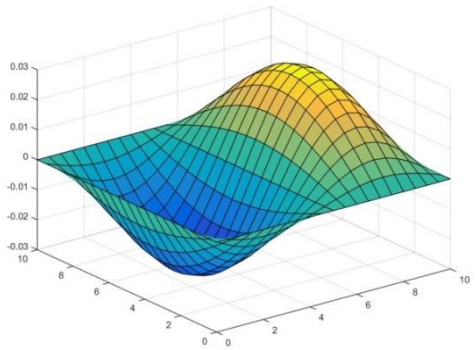

(d)

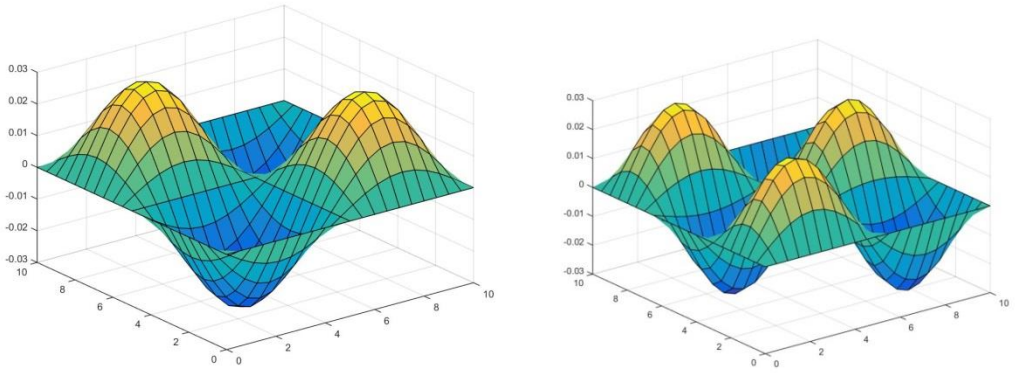

(e) (f)

Figure 4.22. First six mode shapes of simply supported CNTRC plate resting on the Pasternak elastic foundation for free vibration

Table 4.17: Dimensionless natural frequency of CNTRC plate with and without elastic foundation

β_w	β_s		V^*_{CNT} = 0.11				V^*_{CNT} = 0.14				V^*_{CNT} = 0.17			
			UD	**X**	**O**	**V**	**UD**	**X**	**O**	**V**	**UD**	**X**	**O**	**V**
0	0	Present[@]	0.1355	0.1469	0.1134	0.1245	0.1436	0.1541	0.1213	0.1328	0.1683	0.1819	0.1409	0.1544
		Present[*]	0.1305	0.1389	0.1107	0.1224	0.1372	0.1443	0.1179	0.1297	0.1622	0.1714	0.1381	0.1520
		Present[$]	0.1335	0.1468	0.1132	0.1246	0.1436	0.1540	0.1211	0.1328	0.1683	0.1818	0.1408	0.1545
		Present[&]	0.1359	0.1473	0.1131	0.1248	0.1440	0.1546	0.1211	0.1332	0.1688	0.1824	0.1408	0.1548
		Ref (2015)	0.1355	0.1469	0.1134	0.1245	0.1436	0.1541	0.1213	0.1328	0.1683	0.1819	0.1409	0.1544
		Ref (2015)	0.1357	0.1472	0.1132	0.1246	0.1438	0.1545	0.1211	0.1329	0.1685	0.1821	0.1408	0.1546
100	0	Present[@]	0.1388	0.1500	0.1173	0.1281	0.1467	0.1570	0.1250	0.1362	0.1710	0.1443	0.1441	0.1573
		Present[*]	0.1336	0.1417	0.1145	0.1259	0.1401	0.1469	0.1215	0.1329	0.1647	0.1736	0.1412	0.1547
		Present[$]	0.1388	0.1498	0.1172	0.1282	0.1467	0.1569	0.1248	0.1362	0.1710	0.1842	0.1440	0.1574
		Present[&]	0.1392	0.1504	0.1171	0.1284	0.1471	0.1575	0.1248	0.1365	0.1714	0.1848	0.1440	0.1577
		Ref (2015)	0.1388	0.1500	0.1173	0.1281	0.1467	0.1570	0.1250	0.1362	0.1710	0.1443	0.1441	0.1573
		Ref (2015)	0.1390	0.1503	0.1172	0.1282	0.1469	0.1574	0.1248	0.1363	0.1712	0.1846	0.1439	0.1574
100	50	Present[@]	0.1683	0.1775	0.1509	0.1594	0.1746	0.1833	0.1567	0.1657	0.1953	0.2070	0.1721	0.1834
		Present[*]	0.1609	0.1665	0.1472	0.1558	0.1658	0.1703	0.1522	0.1610	0.1874	0.1942	0.1686	0.1798
		Present[$]	0.1682	0.1773	0.1507	0.1594	0.1745	0.1832	0.1566	0.1658	0.1952	0.2070	0.1721	0.1834
		Present[&]	0.1685	0.1778	0.1506	0.1596	0.1749	0.1837	0.1566	0.1660	0.1956	0.2075	0.1721	0.1837
		Ref (2015)	0.1683	0.1775	0.1509	0.1594	0.1746	0.1833	0.1567	0.1657	0.1953	0.2070	0.1721	0.1834
		Ref (2015)	0.1683	0.1777	0.1507	0.1595	0.1747	0.1836	0.1566	0.1659	0.1954	0.2073	0.1720	0.1835

Present[@]- Analytical non-polynomial shear deformation theory based on secant function.
Present[*]- Analytical non-polynomial shear deformation theory based on inverse hyperbolic sine function.
Present[$]- FE modeling using non-polynomial shear deformation theory based on secant function.
Present[&]- FE modeling using non-polynomial shear deformation theory based on inverse hyperbolic sine function.
[Ref (2015)]-Wattanasakulpong and Chaikittiratana (2015)

4.4.3.2. Buckling analysis of bi-axially loaded functionally graded Carbon nanotube reinforced composite plates resting on Pasternak elastic foundation

In this section, the dimensionless critical buckling load subjected to bi-axial compressive load (Ψ_x= -1, Ψ_y= -1) of CNTRC plate with and without Pasternak elastic foundation is shown in Table 4.18. For the analysis of non-dimensional buckling load of the simply supported carbon nanotube reinforced composite plate resting on Pasternak's elastic foundation, different distribution of carbon nanotube reinforcement pattern is selected from Table 3.1. The material property selected here, is given in Table 3.3 and the non-dimensional parameter selected sub section 3.11. The presented results of dimensionless critical buckling loads are achieved using the analytical and FE methods in the framework of non-polynomial shear deformation theories, which is based on the secant function and inverse hyperbolic sine function. The presented dimensionless critical buckling loads are compared with the available results which were given by Wattanasakulpong and Chaikittiratana (2015). It is observed that the present results are agreed well with the available result for side to thickness ratio of 10. From the table it is also observed that, the FG-X reinforcement distribution of CNTs in the composite plate with and without Pasternak elastic foundation resist the uniaxial compressive load very well by giving the maximum value of dimensionless critical buckling load which is followed by UD and FG-O reinforcement distribution. The influence of the Winkler spring constant factors and shear layer spring constant factors on the non-dimensional critical buckling load can be observed from the table, the Winkler spring constant factors and shear layer spring constant factors increases, with the increase in the stiffness of the system in the lateral direction due to which the dimensionless critical buckling load increases for the CNTRC plate with Pasternak's elastic foundation. The stiffness of the system in the lateral direction can also be increased by increasing the

volume fraction of CNTs in the composite plate for which the dimensionless critical buckling load increases for the CNTRC plate with Pasternak elastic foundation.

First six buckling mode shapes of simply supported CNTRC plate resting on the Pasternak elastic foundation are shown in Figure 4.24. The buckling mode shapes are drawn for the FG-X distribution of CNTs with volume fraction of CNTs as 0.17 and side to thickness ratio of 10. The Winkler springs constant factors and shear layer spring constant factors is selected as 100 and 50, respectively. This analysis is carried out using the analytical approach implementing the secant function based non-polynomial shear deformation theory.

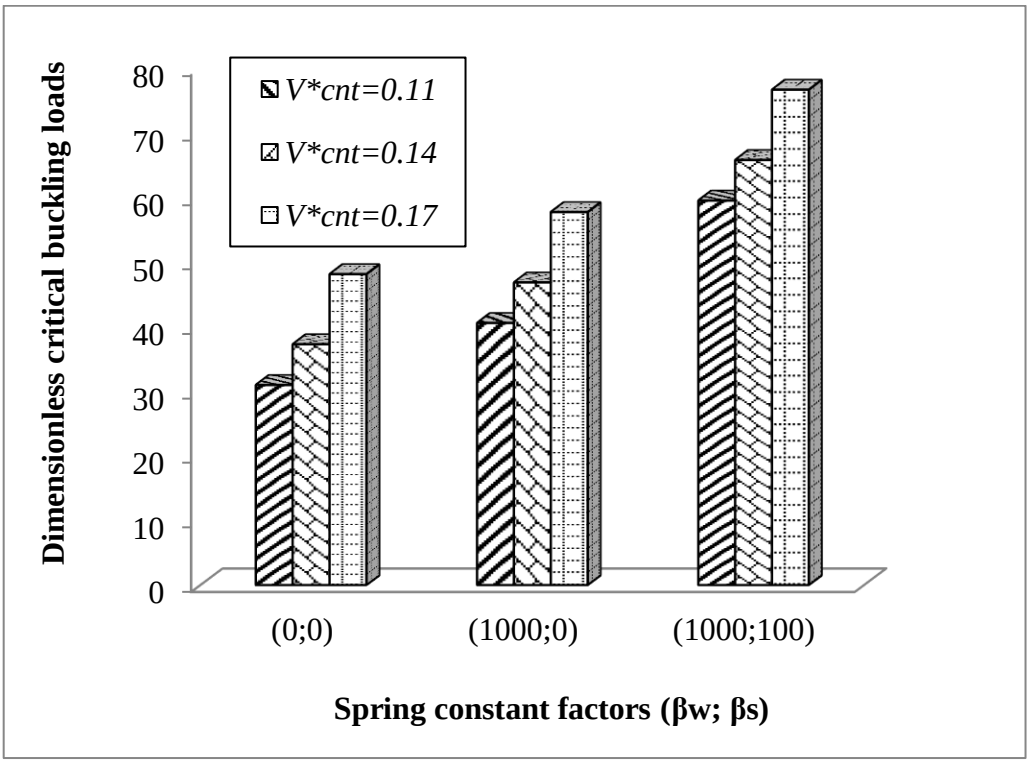

Figure 4.23. Effect of different spring constant factors on non-dimensional critical buckling load under uni-axial loading (Ψ_x= -1, Ψ_y= 0) condition for different volume fraction of CNTs

Table 4.18: Dimensionless critical buckling load under uniaxial compressive load (Ψ_x= -1, Ψ_y= 0) of CNTRC plate with and without elastic foundation

β_w	β_s		V^*_{CNT} = 0.11			V^*_{CNT} = 0.14			V^*_{CNT} = 0.17		
			UD	**X**	**O**	**UD**	**X**	**O**	**UD**	**X**	**O**
0	0	Present[@]	20.6812	24.2858	14.4994	23.3556	26.8936	16.6988	32.3177	37.6938	22.6828
		Present[*]	21.0820	25.0167	14.4132	23.8919	27.7528	16.6223	32.9265	38.6099	22.6197
		Present[$]	20.6777	24.2339	14.4490	23.3451	26.8367	16.6450	32.3136	37.6522	22.6469
		Present[&]	20.7952	24.4251	14.4314	23.4968	27.0580	16.6426	32.4930	37.9061	22.6581
		Ref (2015)]	20.6814	24.2864	14.4990	22.3559	26.8941	16.6984	32.3180	37.6944	22.6823
		Ref (2015)]	20.7286	24.3943	14.4515	23.4229	27.0177	16.6451	32.3890	37.8069	22.6276
100	0	Present[@]	21.7078	25.3424	15.5260	24.3822	27.9200	17.7254	33.3443	38.7204	23.7094
		Present[*]	22.1086	24.0433	15.4398	24.9185	28.7794	17.6489	33.9531	39.6365	23.6463
		Present[$]	21.7043	25.2604	15.4763	24.3717	27.8633	17.6716	33.3402	38.6788	23.6735
		Present[&]	21.8217	25.4516	15.4579	24.5233	28.0845	17.6691	33.5195	38.9326	23.6846
		Ref (2015)]	21.7080	25.3130	15.5256	24.3825	27.9207	17.7250	33.3446	38.7210	23.7089
		Ref (2015)]	21.7552	25.4209	15.4781	24.4495	28.0443	17.6717	33.4156	38.8335	23.6542
100	50	Present[@]	31.8399	34.4445	25.6581	34.5143	38.0521	27.8576	43.4764	48.8525	33.8415
		Present[*]	32.2407	36.1754	25.5719	35.0506	38.9115	27.7810	44.0852	49.7686	33.7784
		Present[$]	31.8364	35.3926	25.6084	34.5038	37.9954	27.8037	43.4723	48.8109	33.8056
		Present[&]	31.9538	35.5837	25.9500	34.6554	38.2166	27.8012	43.6516	49.0647	33.8168
		Ref (2015)]	31.8401	35.4451	25.6577	34.5146	38.0528	27.8571	43.4768	48.8531	33.8410
		Ref (2015)]	31.8873	35.5531	25.6102	34.5816	38.1764	27.8038	43.5477	48.9656	33.7863

Table 4.19: Dimensionless critical buckling load under bi axial compressive load (Ψ_x= -1, Ψ_y= -1) of CNTRC plate with and without elastic foundation

β_w	β_s		V^*_{CNT} = 0.11			V^*_{CNT} = 0.14			V^*_{CNT} = 0.17		
			UD	**X**	**O**	**UD**	**X**	**O**	**UD**	**X**	**O**
0	0	Present[@]	10.3406	12.1429	7.2497	11.6788	13.4467	8.3494	16.1588	18.8469	11.3414
		Present[*]	10.5410	12.5084	7.2066	11.9460	13.8764	8.3112	16.4633	19.3050	11.3098
		Present[$]	10.3406	12.1430	7.2496	11.6784	13.4469	8.3493	16.1589	18.8470	11.3413
		Present[&]	10.4526	12.3528	7.2161	11.8287	13.6926	8.3168	16.3289	19.1042	11.3118
		Ref (2015)]	10.3407	12.1432	7.2495	11.6780	13.4471	8.3492	16.1590	18.8472	11.3412
		Ref (2015)]	10.3643	12.1972	7.2257	11.7115	13.5089	8.3225	16.1945	18.9035	11.3138
100	0	Present[@]	10.8539	12.6562	7.7630	12.1911	13.9600	8.8627	16.6721	19.3602	11.8547
		Present[*]	11.0543	13.0217	7.7199	12.4593	14.3890	8.8245	16.9766	19.8183	11.8231
		Present[$]	10.8539	12.6563	7.7629	12.1912	13.9602	8.8626	16.6722	19.3603	11.8545
		Present[&]	10.9659	12.8661	7.7294	12.3420	14.2056	8.8301	16.8422	19.6175	11.8251
		Ref (2015)]	10.8540	12.6565	7.7628	12.1913	13.9604	8.8625	16.6723	19.3605	11.8544
		Ref (2015)]	10.8776	12.7105	7.7390	12.2248	14.0222	8.8358	16.7078	19.4168	11.8271
100	50	Present[@]	15.9199	17.7222	12.8291	17.2571	19.0261	13.9288	21.7382	24.4263	16.9208
		Present[*]	16.1204	18.0877	12.7859	17.5353	19.4557	13.8905	22.0426	24.8843	16.8892
		Present[$]	15.9200	17.7100	12.8290	17.2572	19.0262	13.9286	21.7383	24.4264	16.9206
		Present[&]	16.0320	17.9321	12.7955	17.4166	19.2719	13.8962	21.9082	24.6835	16.8911
		Ref (2015)]	15.9201	17.7226	12.8289	17.2573	19.0264	13.9285	21.7384	24.4265	16.9205
		Ref (2015)]	15.9437	17.7765	12.8051	17.2980	19.0882	13.9019	21.7739	24.4828	16.8931

Present[@]- Analytical non-polynomial shear deformation theory based on secant function.
Present[*]- Analytical non-polynomial shear deformation theory based on inverse hyperbolic sine function.
Present[$]- FE modeling using non-polynomial shear deformation theory based on secant function.
Present[&]- FE modeling using non-polynomial shear deformation theory based on inverse hyperbolic sine function.
[Ref (2015)]-Wattanasakulpong and Chaikittiratana (2015).

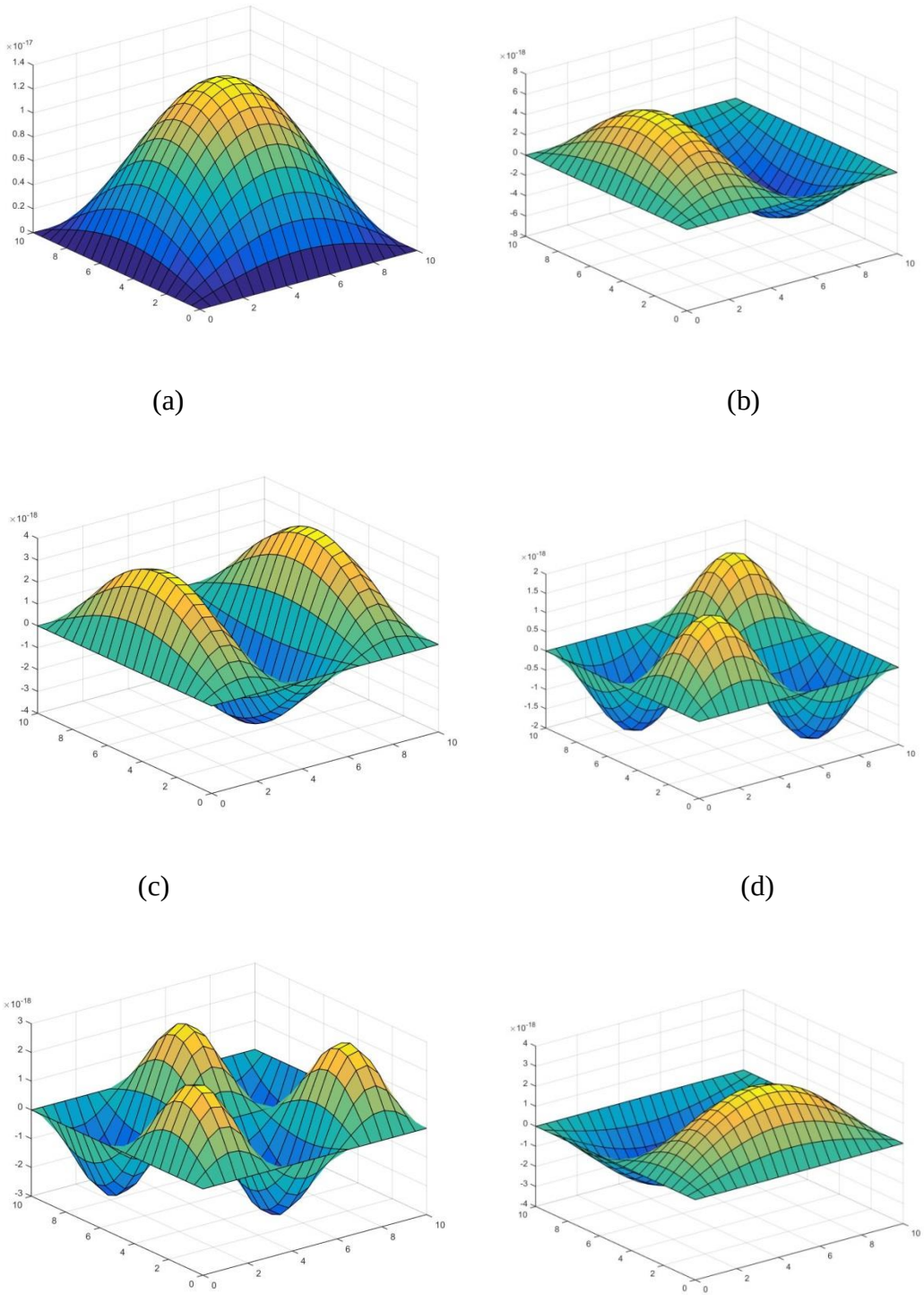

(a) (b)

(c) (d)

(e) (f)

Figure 4.24. First six mode shapes of simply supported CNTRC plate resting on the Pasternak elastic foundation for buckling loads

4.5. Closure

Detailed investigations on carbon nanotube reinforced composite plate structures are presented in this chapter. Different problems of carbon nanotube reinforced composite plate structures supported with and without elastic medium have been solved which would be beneficial for future research work. The performance of the present non-polynomial shear deformation theories based on secant function and inverse hyperbolic sine function are verified against several existing plate models available in the literature. The comparison of the present responses with the established results indicates the accuracy and efficiency of the present analytical and FE formulations. It is found that the present responses are in close agreement with established results and are found to yield efficient static and dynamic responses of both carbon nanotube reinforced composite plate structures. The secant function and inverse hyperbolic sine function used in the model for refining the bending behavior of the plate structures and the satisfaction of the traction free boundary conditions of transverse shear stresses are the two primary features of the present model which are responsible for the better performance of the present model over the existing models.